VIBRATION CONTROL OF A SMART CURVED BEAM WITH VARIABLE CURVATURE

A Thesis Submitted to
the Graduate School of Engineering and Sciences of
İzmir Institute of Technology
in Partial Fulfillment of the Requirements for the Degree of

MASTER OF SCIENCE

in Mechanical Engineering

by
Ali Vâlâ KAVUNCU

December 2017
İZMİR

We approve the thesis of **Ali Vâlâ KAVUNCU**

Examining Committee Members:

Prof. Dr. Bülent YARDIMOĞLU
Department of Mechanical Engineering, İzmir Institute of Technology

Prof. Dr. Serhan ÖZDEMİR
Department of Mechanical Engineering, İzmir Institute of Technology

Prof. Dr. Zeki KIRAL
Department of Mechanical Engineering, Dokuz Eylul University

27 December 2017

Prof. Dr. Bülent YARDIMOĞLU
Supervisor, Department of Mechanical Engineering,
İzmir Institute of Technology

Prof. Dr. Metin TANOĞLU
Head of the Department of
Mechanical Engineering

Prof. Dr. Aysun SOFUOĞLU
Dean of the Graduate School
of Engineering and Sciences

ACKNOWLEDGEMENTS

I would like to express my deep gratitude to my supervisor Prof. Dr. Bülent YARDIMOGLU for his valuable guidance. His contributions and advice were indispensable. I was undoubtedly serendipitous to receive such unreserved attention.

I would also like to thank my parents for their encouragement during my study. Experience they provided helped me instill a balance of my studies and my profession.

Last but definitely not least, I would like to assert my special thanks and gratefulness to my wife for her selfless support. Without her support in every stage of my studies and encouragement when greatly needed, this study would have not been possible.

ABSTRACT

VIBRATION CONTROL OF A SMART CURVED BEAM
WITH VARIABLE CURVATURE

In this study, vibration control of smart curved beam with variable curvature under in plane vibration is studied. The current problem is mathematically represented by differential eigenvalue problem with variable coefficients. Since the solution of these types of problem is based on the functions of the variable coefficients, Finite Element Method is used to reduce the differential eigenvalue problem to discrete eigenvalue problem. A computer code is developed in ANSYS to model the geometry and solve the vibration control problem by using APDL (ANSYS Parametric Design Language). Vibration control is performed by displacement feed-back algorithm. The effects of control parameters on time response are investigated.

ÖZET

DEĞİŞKEN EĞRİLİKLİ AKILLI EĞRİ ÇUBUKLARIN TİTREŞİM KONTROLU

Bu çalışmada, düzlem içindeki titreşim altında olan değişken eğriliğe sahip akıllı eğri kirişin titreşim kontrolü incelenmiştir. Mevcut problem, matematiksel olarak değişken katsayılı diferansiyel özdeğer problemi ile temsil edilmektedir. Bu problem tiplerinin çözümü değişken katsayıların fonksiyonlarına bağlı olduğundan, diferansiyel özdeğer problemini ayrık özdeğer problemine indirgemek için Sonlu Elemanlar Metodu kullanılmaktadır. ANSYS'de, geometriyi modellemek ve titreşim kontrol problemini çözmek için APDL (ANSYS Parametrik Tasarım Dili) kullanarak bir bilgisayar kodu geliştirilmiştir. Titreşim kontrolü yer değiştirme geri besleme algoritması ile gerçekleştirilmiştir. Kontrol parametrelerinin zaman cevabı üzerindeki etkileri araştırılmıştır.

TABLE OF CONTENTS

LIST OF FIGURES

Figure **Page**

LIST OF TABLES

Table **Page**

LIST OF SYMBOLS

a	coefficient of parabola
$\vec{a}$	acceleration vector
A	cross-sectional area
A_p	cross-sectional area of piezoelectric patch
b	width
b_p	width of piezoelectric patch
$[C]$	structural damping matrix
D	electric displacement
d	piezoelectric strain coefficient
E	Young's modulus, electric field
E_p	Young's modulus of piezoelectric material
$\vec{F}$	force vector
F_p	force due to piezoelectric patch
$\{F\}$	nodal force vector
G	transfer function of system
G_s	transfer function of smart beam
h	radial distance of piezoelectric patch
I	second moment of area
k	piezoelectric coupling coefficient
K_c	transfer function of controller
K_p	combined transfer function
K_s	transfer function of voltage sensor
K_v	transfer function of voltage amplifier
$[K]$	structural stiffness matrix
$[K^d]$	dielectric conductivity matrix
$[K^z]$	piezoelectric coupling matrix
L_p	length of piezoelectric patch
$\{L\}$	nodal charge vector
M_y	internal moment about y-axis
M_{yp}	bending moment about y-axis due to piezoelectric patch
m_y	distributed moment about y-axis

m_{yp}	distributed bending moment about y-axis due to piezoelectric patch
M_i	moment about i-axis
$[M]$	structural mass matrix
m	mass per unit length, mass
N	internal shear force
q_n	distributed normal force
q_t	distributed tangential force
q_{tp}	piezoelectric applied distributed force
$R(s)$	radius of curvature
S	strain
s	spatial variable, mechanical compliance
t	time
t_p	thickness of piezoelectric patch
T	internal normal force, applied stress
u	radial displacement
$\{u\}$	nodal displacement vector
V	elastic strain energy, applied voltage
$\{V\}$	nodal electric potential vector
w	tangential displacement
$(\grave{})$	derivative with respect to spatial variable
$(\ddot{})$	second derivative with respect to time
α	mass matrix multiplier
$\vec{\alpha}$	angular acceleration vector
β	stiffness matrix multiplier
ε	strain normal to the cross-section, dielectric permittivity
κ_0, $\kappa(s)$, k_0, $k(s)$	curvature; constant, variable, at s=0, variation function
κ_1'	curvature after displacement
ρ	density of beam material
ρ_o	initial radius of curvature
ω	natural frequency

CHAPTER 1

GENERAL INTRODUCTION

Curved beams are interesting structural members due to their deformation behaviors. They can be seen in numerous engineering applications as main or complimentary components such as stiffeners in different types of structure, for example: airplanes and ships.

Curved beams can be categorized depending on their shapes. In first approach, it may be planar or spatial beams. In second, curvature of curved beams can be used for classification as circular and non-circular. Then, cross-section of the curved beam can be considered. They may have uniform cross-section or varying cross-section along its circumferential axis. Moreover, material characteristic of the curved beams can be a criterion for classification. They may be isotropic, orthotropic, or composite.

Many researchers studied on smart curved beams. However, studies on smart curved beams with variable curvature are limited.

Brei and Blechschmidt (1992) designed a semicircular polymeric piezoelectric actuator shown in Figure 1.1. They used bimorph form of piezoelectric materials. They modeled the system as deflection and force models. They found that a bimorph semicircular cantilever beam produces significantly more force than a straight bimorph cantilever beam having the same length.

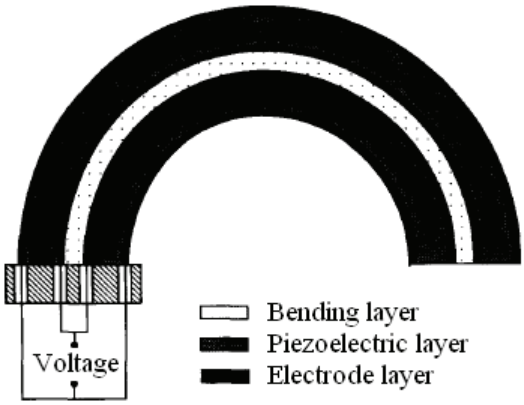

Figure 1.1. Microactuator design of semicircular cross section
(Source: Brei and Blechschmidt 1992)

Brei (1995) described C-Block actuators in the shape of a semicircle, as shown in Figure 1.2, in order to arrange it as series, arrays, and parallel which are shown in Figure 1.3. He presented mathematical force model, manufacturing techniques and experimental verification of force performance of C-Blocks.

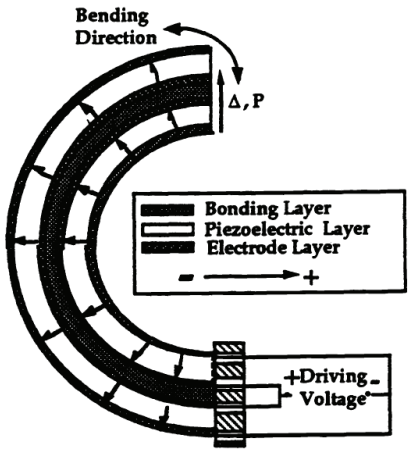

Figure 1.2. Piezoelectric C-block actuator
(Source: Brei 1995)

(a) Series architecture

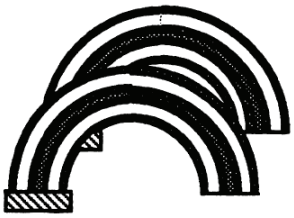

(b) Parallel architecture

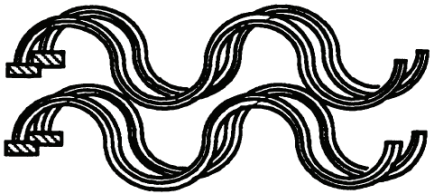

(c) Distributed array architecture

Figure 1.3. Different piezoelectric C-Block actuator architectures
(Source: Brei 1995)

Banks and Zhang (1997) developed a computational procedure to approximate the solutions of a mathematical model of the vibrations of a curved beam including pairs of piezoceramic patches as passive or as active devices. They used Galerkin approximation with hybrid B-spline basis elements. Their model is given in Figure 1.4.

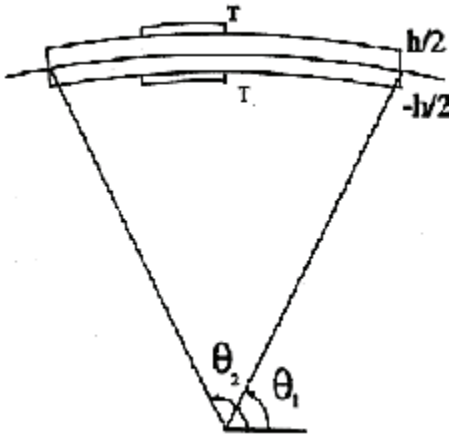

Figure 1.4. Curved beam with pairs of piezoceramic patches
(Source: Banks and Zhang 1997)

Moskalik and Brei (1997) extended former studies for deflection-voltage model of multilayered piezoelectric curved beams, as shown in Figure 1.5, consisting of a variable number of active or inactive layers. Moskalik and Brei (1997) also studied on their C-block actuators for force-deflection behavior of the system.

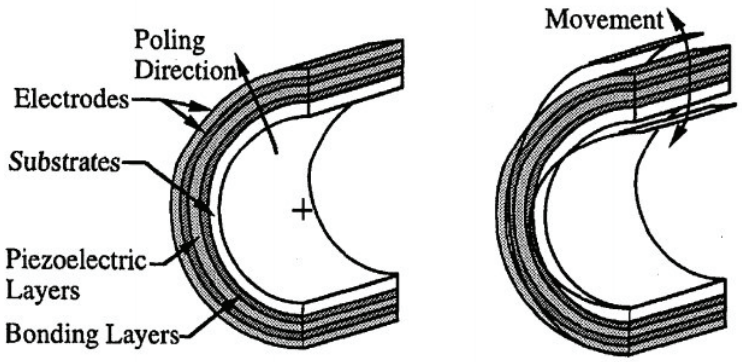

Figure 1.5. Polymeric piezoelectric multilayered C-block
(Source: Moskalik and Brei 1997)

Shih (2000) studied on vibration control piezoelectric laminated curved beam with distributed sensing and actuating systems shown in Figure 1.6. He derived the sensing and control equations in continuous domain by modal expansion method and investigated the design parameters such as thickness of sensor, actuator, and beam.

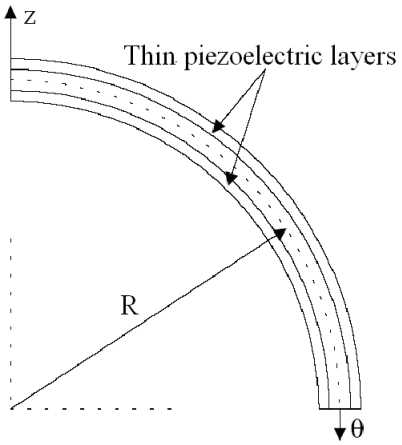

Figure 1.6. A curved beam with bonded piezoelectric patches
(Source: Shih 2000)

Sun and Tong (2002) presented a mathematical model for thin-walled curved beams with piezoelectric actuator and sensor patches shown in Figure 1.7. They investigated the effect of debonding piezoelectric patches on vibration control as open- and closed-loop. They showed a significant side effect of edge debonding of the piezoelectric patch on the closed-loop control of the curved beams.

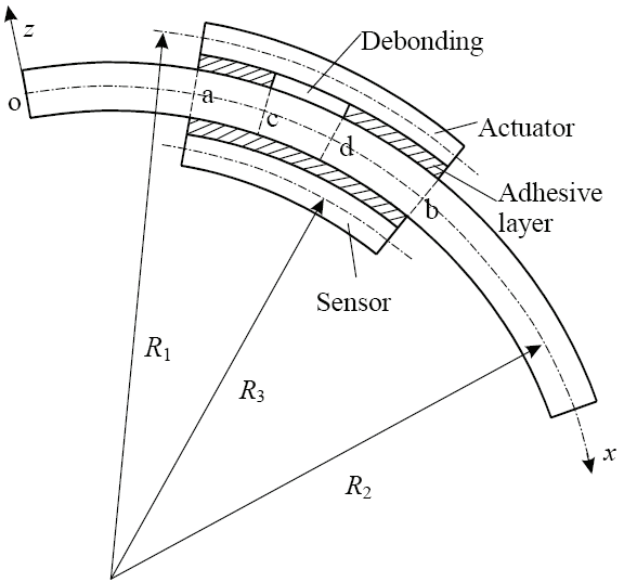

Figure 1.7. A curved beam with debonded piezoelectric patches
(Source: Sung and Tong 2002)

Yoon et al. (2005) revisited the design of an energy harvesting shoe insert which is a curved piezoelectric unimorph beam. They used shallow thin shell theory of Donnell-Mushtari, composite laminate theory, and linear piezoelectric constitutive equations.

Kuang et al (2007) analyzed the static responses of a circular curved beam bonded with a single piezoelectric actuator or symmetric actuators as shown in Figure 1.8. They adopted the equilibrium equation of curved beam given by Love (1944) and Henrych (1981) for piezolaminated circular beams. Their assumptions can be summarized as follows:

- Inextensionality condition only for the bimorph curved beam due to the symmetric piezoelectric layers,
- No shear deformation, moment of inertia and tangential inertia force,
- No debonding,
- Continuous strains along the radial direction of the piezolaminated beam,
- Constant electric field along the radial direction due to thin piezoelectric actuator.

They also studied on the control parameters of a cantilever circular curved beam for displacement control. For the control problem of a cantilever bimorph curved beam, a very high radial load is acted at an arbitrary location of the beam. However, for the control problem of a cantilever unimorph curved beam, a radial load is acted at the free end. They found the optimum length and location of the actuators.

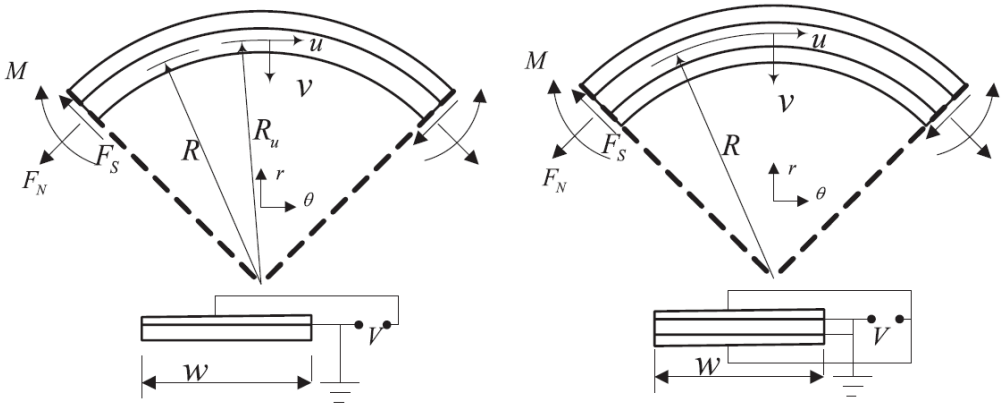

(a) (b)

Figure 1.8. The circular unimorph (a) and bimorph (b) curved beams
(Source: Kuang et al 2007)

Wang (2010) formulated the Timoshenko curved beam having a pair of piezoelectric segments that is shown in Figure 1.9. In order to study on responses of the smart curved beam system under either an external force at the tip of the beam or an applied voltage on the actuator, the analytical-transfer matrix method is employed.

The effects of length, thickness and location of the piezoelectric pair on the responses of the curved beam system are presented.

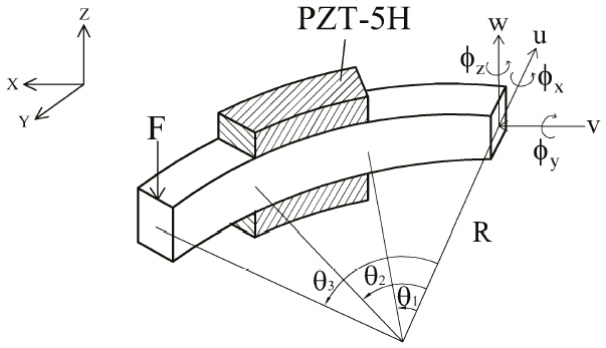

Figure 1.9. A curved beam with bonded piezoelectric patches
(Source: Wang 2010)

In this study, a curved beam with variable curvature under in plane vibration is considered. In order to apply vibration control to this beam, a unimorph piezoelectric patch is bonded. The present case is mathematically represented by differential eigenvalue problem with variable coefficients. Since the solutions of these types of problem are based on the functions of the variable coefficients, Finite Element Method is used to reduce the differential eigenvalue problem to discrete eigenvalue problem. A computer code is developed in ANSYS to model the geometry and solve the vibration control problem by using APDL (ANSYS Parametric Design Language). Vibration control is performed by displacement feed-back algorithm. The effects of control parameters on time response are investigated.

CHAPTER 2

THEORETICAL ANALYSIS

2.1. Introduction

In this chapter, as first step, the axis of curved beam is given mathematically. After this, derivation of equation of motion is presented by using Love's approach (Love, 1944). Due to the usage of piezoelectric material for vibration control, piezoelectric materials and constitutive equations are introduced in reasonable detail. Then, piezoelectric layer effect on equations of motion of the curved beam system is formulated. Finite element modeling of host beam and piezoelectric patch in ANSYS are outlined. The concept of natural frequencies and the time response of discrete structure are summarized. Finally, active vibration control procedure is explained.

2.2. Axis of the Curved Beam

The parabola illustrated in Figure 2.1 is selected as axis of curved beam to form it with variable curvature. In order to eliminate the confusion regarding sign convention in equation of motion, the coordinate system used by Love (1944) is considered to express the mathematical expression of parabola in the *z*-*x* plane.

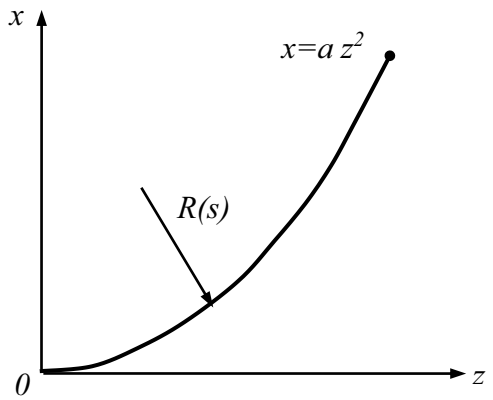

Figure 2.1. The parabola and its parameters

Mathematical expression of the parabola is given as

$$x = az^2 , \quad z > 0 \tag{2.1}$$

The curvature κ of a point on the curve is written as follows:

$$\kappa = \frac{\frac{d^2x}{dz^2}}{\left[1 + (dx/dz)^2\right]^{3/2}} \tag{2.2}$$

If Equation (2.1) is substituted into Equation (2.2), it gives:

$$\kappa = \frac{\frac{d^2}{dz^2}(az^2)}{\left[1 + \left[\frac{d}{dz}(az^2)\right]^2\right]^{3/2}} \tag{2.3}$$

and then, by simplifying;

$$\kappa = \frac{2a}{\left[1 + 4a^2z^2\right]^{3/2}} \tag{2.4}$$

Equation (2.4) gives the curvature at any abscissa z for the selected parabola.

2.3. Equation of Motion by Newtonian Method

Newtonian method is based on the following two vectorial equations with usual notation:

$$\sum_i \vec{F}_i = m\vec{a} \tag{2.5}$$

$$\sum_i \vec{M}_i = I\vec{\alpha} \tag{2.6}$$

A curved beam with arbitrary curvature is shown in Figure 2.2 by introducing the internal normal force T, internal shear force N, and internal bending moment M_y.

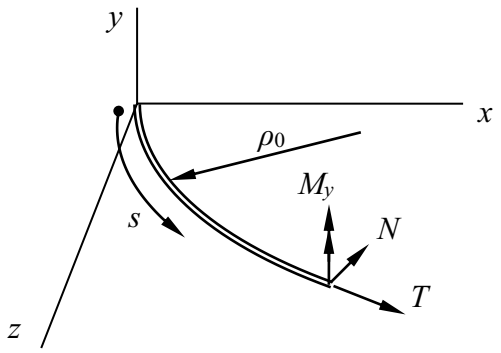

Figure 2.2. Internal forces and moment of curved beam

The internal normal force T is written as

$$T = E\,A\,\varepsilon \tag{2.7}$$

where E is the modulus of elasticity, A is the cross-sectional area of the curved beam, and ε is the strain normal to the cross-section due to tension and is given by Love (1944)

$$\varepsilon = \frac{dw}{ds} - \kappa_0' u \tag{2.8}$$

where u and w are displacements of any point on curved beam axis in radial and circumferential directions, respectively. Also, κ_0' is the initial curvature of the curved beam axis which lies in the x-z plane.

In order to express the internal normal force T in terms of displacements, Equation (2.8) is substituted into Equation (2.7), and then the following equation is written

$$T = E\,A\left(\frac{dw}{ds} - \kappa_0' u\right) \tag{2.9}$$

The internal bending moment M_y about the y axis is written as (Love, 1944)

$$M_y = EI\,(\kappa_1' - \kappa_0') \tag{2.10}$$

where I is second moment of area of the cross-section of the curved beam about y axis. Also, κ_1' is dynamic curvature in x-z plane which is given by Love (1944) as

$$\kappa_1' = \kappa_0' + \frac{d}{ds}\left(\frac{du}{ds} + \kappa_0'\, w\right) \tag{2.11}$$

In order to express the internal bending moment M_y in terms of displacements, Equation (2.11) is substituted into Equation (2.10), and then the following equation is written

$$M_y = EI\left(\frac{d}{ds}\left(\frac{du}{ds} + \kappa_0'\, w\right)\right) \tag{2.12}$$

The internal shear force N can be treated as the derivative of the internal bending moment M_y .

Neglecting the rotary inertia, equations of motion of the curved beam are obtained by using Equations (2.5) and (2.6) as follows:

$$\frac{dN}{ds} + T\kappa_1' + q_t = \rho\, A\, \ddot{u} \tag{2.13}$$

$$\frac{dT}{ds} - N\,\kappa_1' + q_n = \rho\, A\, \ddot{w} \tag{2.14}$$

$$\frac{dM_y}{ds} + N + m_y = 0 \tag{2.15}$$

where ρ is density of material, q_n, q_t are distributed force in normal and tangential directions. Also, m_y is the distributed moment about y axis.

It is clear that Equations (2.13)-(2.16) give non-linear equations. Therefore, higher orders terms are neglected to obtain linear differential equations.

2.4. Piezoelectric Materials and Constitutive Equations

Curie brothers discovered the piezoelectric effects shown in Figure 2.3. They produced piezoelectric material by the polarization process as shown in Figure 2.4. This process is done by heating the material above its Curie temperature and applying a strong electric field. Material looses its spontaneous polarization in Curie temperature.

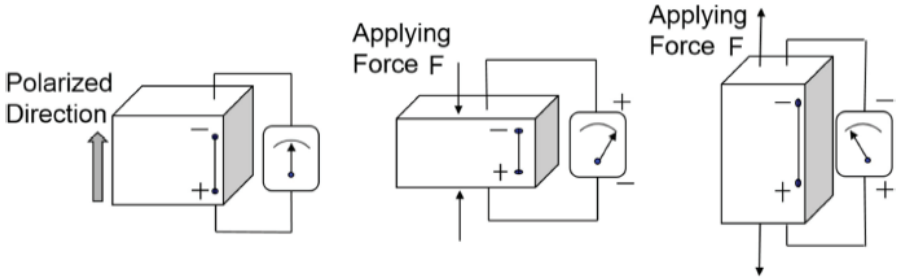

(a) Direct piezoelectric effect

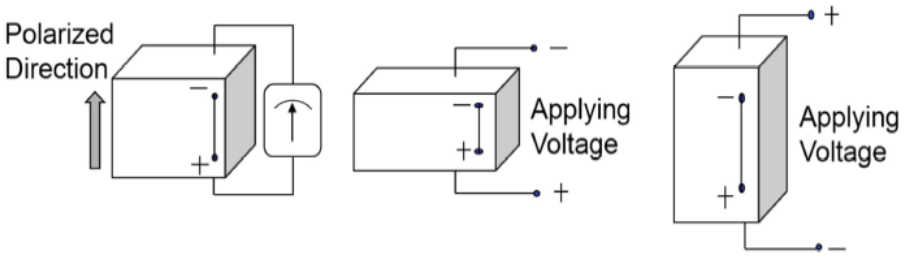

(b) Converse piezoelectric effect

Figure 2.3. Direct and converse piezoelectric effects
(Source: Huo et al 2017)

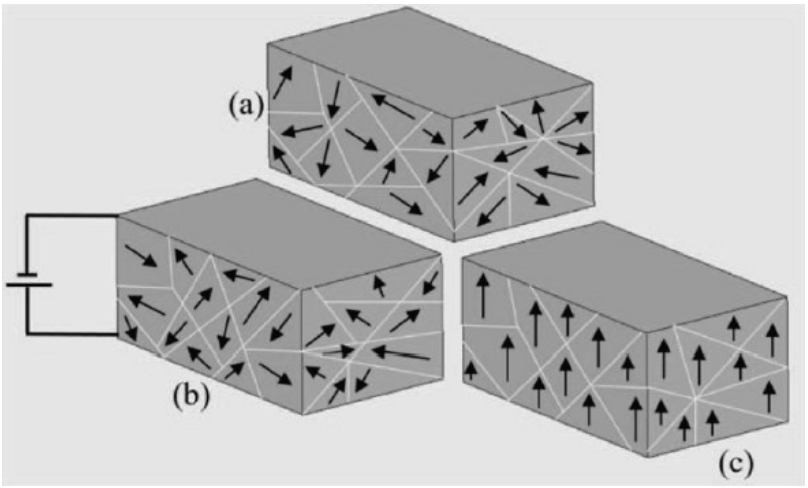

Figure 2.4. Polarization stages (a) before, (b) during (c) after polarization (Source: abdal-Kadhim and Leong 2016)

In order to introduce the constitutive equations of piezoelectric materials, the nomenclature given in the IEEE Standard on Piezoelectricity (1988) is used in this part since the clear textbook written by Leo (2007) has the same notation. One dimensional system is considered first.

Piezoelectric materials exhibit electromechanical coupling so that they are used to design devices for sensing and actuation. The relationship between strain S (m/m) and electric displacement D (C/m^2) as a function of applied stress T (N/m^2) and electric field E (V/m) is given in matrix form by Leo (2007) as

$$\begin{Bmatrix} S \\ D \end{Bmatrix} = \begin{bmatrix} s & d \\ d & \varepsilon \end{bmatrix} \begin{Bmatrix} T \\ E \end{Bmatrix} \tag{2.16}$$

where s (m^2/N) is the reciprocal of the modulus which is called the mechanical compliance, d (C/N) is the piezoelectric strain coefficient, and ε (F/m) is dielectric permittivity of the material.

The top partition of Equation (2.16) is related to the converse piezoelectric effect or electrical-to-mechanical coupling, whereas the bottom partition regarding with the direct effect or mechanical-to-electrical coupling.

Equation (2.16) can be expressed with stress and electric field as the dependent variables and strain and electric displacement as the independent variables as

$$\begin{Bmatrix} T \\ E \end{Bmatrix} = \frac{1}{1-k^2}\begin{bmatrix} s^{-1} & -d^{-1}k^2 \\ -d^{-1}k^2 & \varepsilon^{-1} \end{bmatrix}\begin{Bmatrix} S \\ D \end{Bmatrix} \tag{2.17}$$

where k is called the piezoelectric coupling coefficient and given as

$$k = \frac{d}{\sqrt{s\varepsilon}} \tag{2.18}$$

It is possible to extend the one dimensional system equations to a general one that relates the electromechanical parameters in Equation (2.16) in all three directions. The common coordinate system used for the piezoelectric material is given in Figure 2.5. In this coordinate system, the poling axis of the material is the 3 direction.

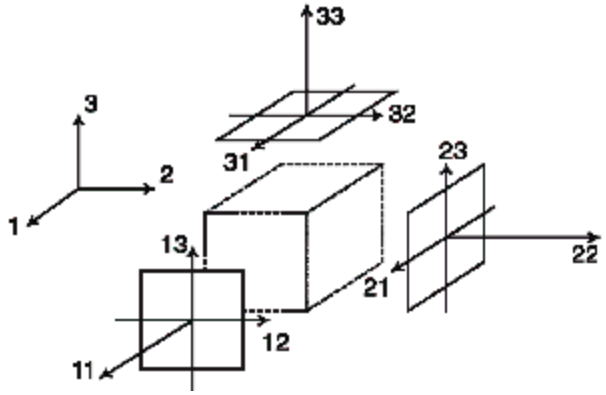

Figure 2.5. The coordinate axes of the piezoelectric material
(Source: Leo 2007)

Many common piezoelectric materials are orthotropic materials. Also, the compliance matrix is symmetric. Moreover, piezoelectric materials have the same elastic modules in the 1 and 2 directions due to the plane of symmetry.

The permittivity matrix is in diagonal form, since the electrical displacements orthogonal to electrical field application direction are not produced. Similarly, some elements of the strain coefficient matrix are zero. Therefore, the constitutive equations of piezoelectric material are obtained in reduced form.

The top partition of Equation (2.16), which is also known as actuation part (Preumont, 2002) due to the electrical-to-mechanical coupling, is written in three dimensions as

$$\begin{Bmatrix} S_1 \\ S_2 \\ S_3 \\ S_4 \\ S_5 \\ S_6 \end{Bmatrix} = \begin{bmatrix} s_{11} & s_{12} & s_{13} & 0 & 0 & 0 \\ s_{12} & s_{22} & s_{23} & 0 & 0 & 0 \\ s_{13} & s_{23} & s_{33} & 0 & 0 & 0 \\ 0 & 0 & 0 & s_{44} & 0 & 0 \\ 0 & 0 & 0 & 0 & s_{55} & 0 \\ 0 & 0 & 0 & 0 & 0 & s_{66} \end{bmatrix} \begin{Bmatrix} T_1 \\ T_2 \\ T_3 \\ T_4 \\ T_5 \\ T_6 \end{Bmatrix} + \begin{bmatrix} 0 & 0 & d_{13} \\ 0 & 0 & d_{23} \\ 0 & 0 & d_{33} \\ 0 & d_{24} & 0 \\ d_{15} & 0 & 0 \\ 0 & 0 & 0 \end{bmatrix} \begin{Bmatrix} E_1 \\ E_2 \\ E_3 \end{Bmatrix} \tag{2.19}$$

The bottom partition of Equation (2.16), which is also known as sensing part (Preumont, 2002) due to the mechanical-to-electrical coupling, is written in three dimensions as

$$\begin{Bmatrix} D_1 \\ D_2 \\ D_3 \end{Bmatrix} = \begin{bmatrix} 0 & 0 & 0 & 0 & d_{15} & 0 \\ 0 & 0 & 0 & d_{24} & 0 & 0 \\ d_{13} & d_{23} & d_{33} & 0 & 0 & 0 \end{bmatrix} \begin{Bmatrix} T_1 \\ T_2 \\ T_3 \\ T_4 \\ T_5 \\ T_6 \end{Bmatrix} + \begin{bmatrix} \varepsilon_{11} & 0 & 0 \\ 0 & \varepsilon_{22} & 0 \\ 0 & 0 & \varepsilon_{33} \end{bmatrix} \begin{Bmatrix} E_1 \\ E_2 \\ E_3 \end{Bmatrix} \tag{2.20}$$

The common operating modes of piezoelectric transducers are 33 and 31 in which second number refers to direction of strain. For 33 operating mode, it is assumed that $T_1=T_2=T_4=T_5=T_6=E_1=E_2=0$. Also, S_1 and S_2 are not main interest. Therefore, the following constitutive equations are needed

$$S_3 = s_{33}^E T_3 + d_{33} E_3 \tag{2.21}$$

$$D_3 = d_{33} T_3 + \varepsilon_{33}^T E_3 \tag{2.22}$$

In Equation (2.21), superscript E represents a short-circuit (E=0) condition. Also, in Equation (2.22), the superscript T denotes a stress-free (T=0) condition.

Similar to 33 operating mode, 31 operating mode can be based on assumption $T_2=T_3= T_4=T_5=T_6=E_1=E_2=0$. Also, S_2 and S_3 are not main interest. Thus, the following constitutive equations are required

$$S_1 = s_{11}^E T_1 + d_{13} E_3 \tag{2.23}$$

$$D_3 = d_{13} T_1 + \varepsilon_{33}^T E_3 \tag{2.24}$$

2.5. Piezoelectric Layer Effect on Equations of Motion

Derivation of the equations of motion of curved beam with variable curvature for in-plane bending is presented in Section 2.3. Equations (2.13), (2.14), and (2.15) have the applied distributed forces q_n, q_t and distributed moment m_y, respectively.

When a thin piezoelectric layer segment is bonded perfectly to concave surface of the curved beam near the root region as shown in Figure 2.6, it applies distributed forces in tangential direction which also generates bending moment about y axis if it is under electrical field. It should be noted that the thin piezoelectric layer segment in Figure 2.6 has light gray color. The applied distributed force q_n due to piezoelectric layer is not effective for 31 operating mode.

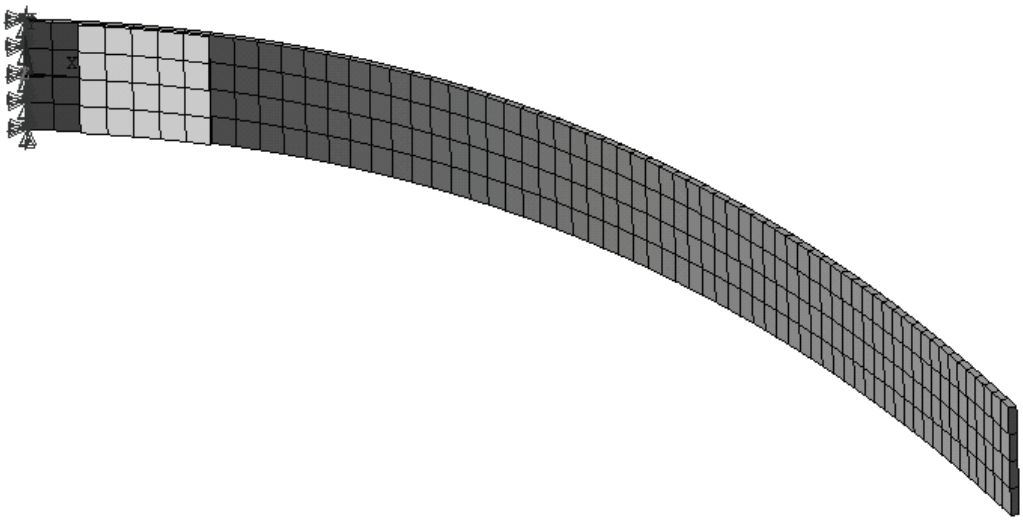

Figure 2.6. Parabolic curved beam with piezoelectric layer segment

Therefore, the applied distributed forces q_{tp} due to piezoelectric layer alone is necessary. To express q_{tp} due to piezoelectric layer, cross-section of the parabolic curved beam with piezoelectric layer segment shown in Figure 2.6 is illustrated in Figure 2.7 with the geometrical parameters. Thus,

$$q_{tp} = F_p / L_p = d_{13} E_p A_p E_3 / L_p \tag{2.25}$$

where L_p is the length of the piezoelectric layer in tangential direction, A_p is the cross-section of the piezoelectric layer and E_p is the Young modulus of the piezoelectric material.

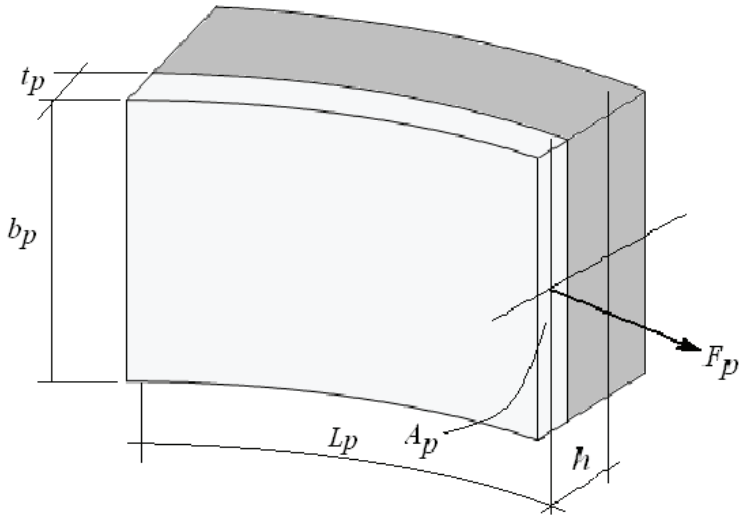

Figure 2.7. The force applied by the piezoelectric layer

Thus, bending moments M_{yp} due to piezoelectric layer is written by using Figure 2.7 as

$$M_{yp} = hF_p \tag{2.26}$$

Thus, distributed bending moment m_{yp} is expressed by using Equation (2.23) as

$$\begin{aligned} m_{yp} &= M_{yp} / L_p \\ &= hF_p / L_p \\ &= h\, d_{13} E_p\, A_p E_3 / L_p \\ &= h d_{13} E_p\, (b_p t_p)(V / t_p) / L_p \\ &= h d_{13} E_p b_p V / L_p \end{aligned} \tag{2.27}$$

2.6. Finite Element Modeling

Finite element method is based on discretization of complex geometrical shapes to simple ones such as lines, triangles, rectangles, tetrahedrons, and rectangular prisms which are called finite elements. This process is called as meshing. Finite elements are connected to each other by their extremities on which element nodes are located. Physical parameters in problems such as displacement, temperature, pressure etc are discretized at the nodes of finite elements. Therefore, an approximate solution function is expressed by using nodal variables. (Yardimoglu, 2012)

The equations of motion of a piezoelectric materials system for one element model are given by Kohnke (2004) as

$$\begin{bmatrix} [M] & [0] \\ [0] & [0] \end{bmatrix} \begin{Bmatrix} \{\ddot{u}\} \\ \{\ddot{V}\} \end{Bmatrix} + \begin{bmatrix} [C] & [0] \\ [0]^T & [0] \end{bmatrix} \begin{Bmatrix} \{\dot{u}\} \\ \{\dot{V}\} \end{Bmatrix} + \begin{bmatrix} [K] & [K^z] \\ [K^z]^T & [K^d] \end{bmatrix} \begin{Bmatrix} \{u\} \\ \{V\} \end{Bmatrix} = \begin{Bmatrix} \{F\} \\ \{L\} \end{Bmatrix} \tag{2.28}$$

where $[M]$ is structural mass, $[C]$ is structural damping matrices. Also, $[K]$, $[K^d]$, and $[K^z]$ are structural stiffness, dielectric conductivity, and piezoelectric coupling matrices, respectively. Details of these matrices are described in Kohnke (2004). It should be noted that a dot above a variable in Equation (2.28) denotes a time derivative as usual.

Moreover, $\{u\}$ and $\{V\}$ in Equation (2.28) are the nodal displacements and nodal electrical potential vectors, respectively. They are written in open form as

$$\{u\} = \{Ux_1 \quad Uy_1 \quad Uz_1 \quad \cdots \quad Ux_n \quad Uy_n \quad Uz_n\}^T \tag{2.29}$$

$$\{V\} = \{V_1 \quad V_2 \quad \cdots \quad V_n\}^T \tag{2.30}$$

Additionally, $\{F\}$ and $\{L\}$ in Equation (2.28) are nodal force and nodal charge vectors, respectively. They are input values of the model.

Finally, the damping matrix $[C]$ is based on Rayleigh's approach which is known as proportional damping.

$$[C] = \alpha[M] + \beta[K] \tag{2.31}$$

where α and β are multipliers for mass and stiffness matrices, respectively.

The assembling of the finite element matrices to obtain the global characteristics such as mass and stiffness are performed by using the continuity conditions.

The finite element model of the smart curved beam is done in ANSYS by employing SOLID45 and SOLID5 for host beam and piezoelectric layer, respectively.

The modeling and solution code is developed by using APDL (ANSYS Parametric Design Language) in ANSYS.

2.7. Natural Frequencies and Time Response

Differential eigenvalue problem is expressed in general form as

$$L[x] = \omega^2 \, M[x] \tag{2.32}$$

where $L[x]$ and $M[x]$ are linear differential operators and ω is eigenvalues.

By using the Finite Element Method, Equation (2.32) is reduced to simultaneous algebraic equations. Boundary conditions are applied to simultaneous algebraic equations in order to obtain the following matrix form

$$[A]\{X\} = \omega^2 \, [B]\{X\} \tag{2.33}$$

Solutions of the generalized eigenvalue problem can be done by using several numerical methods. The available mode-extraction methods in ANSYS are Block Lanczos (default), subspace, PowerDynamics, reduced, unsymmetric, damped, and QR damped.

Time response of the system is also called transient dynamic analysis. ANSYS uses three methods to do a transient dynamic analysis which are

- the full method,
- the mode superposition method,
- the reduced method.

In the full mesthod, the full system matrices are used. However, the mode superposition method sums factored mode shapes found from modal analysis. On the other hand, the reduced method uses master degrees of freedom provided by the user and then reduced matrices.

2.8. Active Vibration Control

Active control of smart structure is accomplished by a displacement feed-back system illustrated in Figure 2.8.

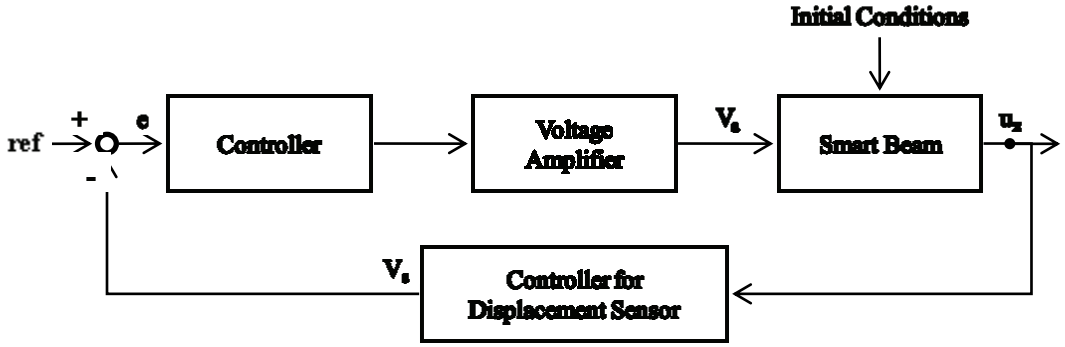

Figure 2.8. Block diagram of the active control system

Active control of smart structure is applied in ANSYS by using transient analysis based on initial displacement of the smart structure. A control loop to apply the actuation voltage is provided by *do-*enddo loop. Within this loop, the error signal is calculated in each time increment depending on the displacement of the smart structure, and then it is amplified for the voltage which will be applied in next time interval. The simulation is continued until desired time.

The transfer function of the active control system shown in Figure 2.1 can be written as

$$G = \frac{u_z}{ref} = \frac{K_c K_v G_s}{1 + K_c K_v K_s G_s} \tag{2.34}$$

where K_c, K_v, and K_s are transfer functions of controller, voltage amplifier and controller for displacement sensor, respectively. G_s is the transfer function of the smart beam. Equation (2.34) can be written by defining $K_p=K_cK_v$ as

$$G = \frac{u_z}{ref} = \frac{K_p G_s}{1 + K_p K_s G_s} \tag{2.35}$$

CHAPTER 3

NUMERICAL RESULTS AND DISCUSSION

3.1. Introduction

The parabolic curved beam axis is formed by the following function:

$$x(z) = 5z^2, \quad (0 \le z \le 0.25) \tag{3.1}$$

The plot of Equation (3.1) is given in Figure 2.1. Cross-sectional dimensions of the curved beam are b=20 mm and h=1.5 mm. It has 0.4463 m arch length. The modeling and solution code is developed by using APDL (ANSYS Parametric Design Language) in ANSYS. Discretizing the parabolic curved beam by the proper number of finite elements which gives the results in desired accuracy, an equivalent circular cantilever beam having the same arch length and cross-section is considered. Natural frequencies of the respective curved beam without piezoelectric layer are found by using different meshes of SOLID45 in ANSYS and the present results are compared with analytical results of Archer (1960). Then, the numbers of finite elements in axial, tangential and radial directions are decided as 4, 96, and 1, respectively.

The piezoelectric layer is modeled by SOLID5 in ANSYS. The meshed parabolic curved beam and piezoelectric layer model is shown in Figure 3.1.

The piezoelectric layer mesh is shaded light grey in Figure 3.1. As seen from the Figure 3.1, the piezoelectric layer is bonded to the concave surface of the parabolic curved beam.

The geometrical properties of the piezoelectric layer are listed below:

Width of the piezoelectric layer b_p=20 mm,
Thickness of the piezoelectric layer t_p=1.5 mm,
Length of the piezoelectric layer s_p=25 mm,
The distance of the piezoelectric layer from the root d_p=10 mm.

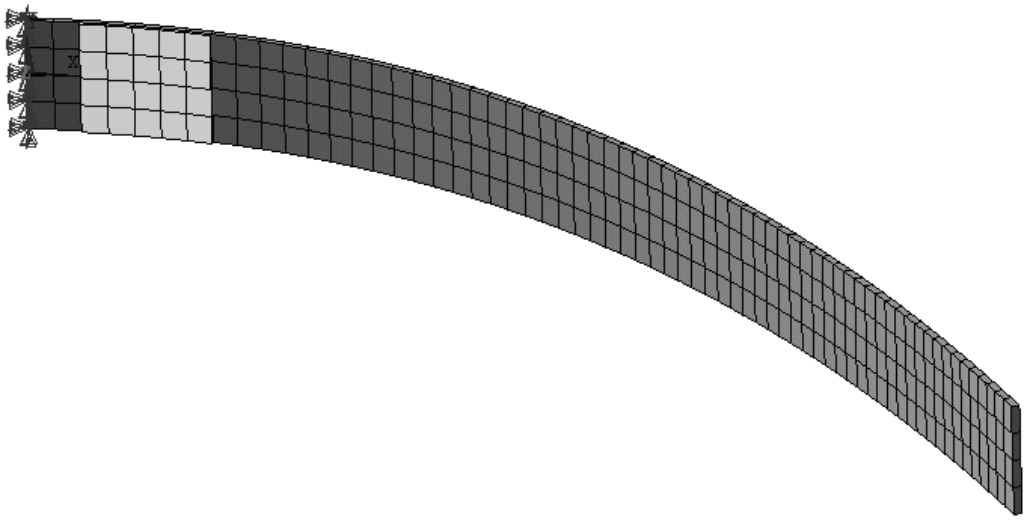

Figure 3.1. The parabolic curved beam and piezoelectric layer after meshing

The material is selected as aluminum for the curved beam of which the properties are given as follows:

Young modulus	68 10^9 N/m^2
Density	2676 kg/m^3
Poisson's ratio	0.32

PZT-5H is used for the piezoelectric layer material. Their material properties are presented in matrix forms as (Auld, 1973),

$$[c^E] = [s^E]^{-1} = \begin{bmatrix} 126 & 79.5 & 84.1 & 0 & 0 & 0 \\ 79.5 & 126 & 84.1 & 0 & 0 & 0 \\ 84.1 & 84.1 & 117 & 0 & 0 & 0 \\ 0 & 0 & 0 & 23.0 & 0 & 0 \\ 0 & 0 & 0 & 0 & 23.0 & 0 \\ 0 & 0 & 0 & 0 & 0 & 23.25 \end{bmatrix} \text{GPa}$$

$$[e] = [d][c] = \begin{bmatrix} 0 & 0 & 0 & 0 & 741 & 0 \\ 0 & 0 & 0 & 741 & 0 & 0 \\ -274 & -274 & 593 & 0 & 0 & 0 \end{bmatrix} \text{C/m}^2$$

$$[\varepsilon^S] = \begin{bmatrix} 1700 & 0 & 0 \\ 0 & 1700 & 0 \\ 0 & 0 & 1470 \end{bmatrix}$$

The numerical matrices are based on IEEE order as [x, y, z, yz, xz, xy]. However, ANSYS uses the order [x, y, z, xy, yz, xz]. Therefore, they must be modified accordingly. Also, [ε^S] is relative permittivity matrix under constant strain condition.

3.2. Parabolic Curved Beam with Piezoelectric Layer

The parabolic smart curved beam introduced in Section 3.1 is used to study on vibration control by displacement feed-back algorithm for different combination of K_p and K_v values.

Time responses of displacement of the mid-point of the tip of the parabolic smart curved beam under displacement feed-back control are given in Figures 3.2-3.18 for K_s=200.

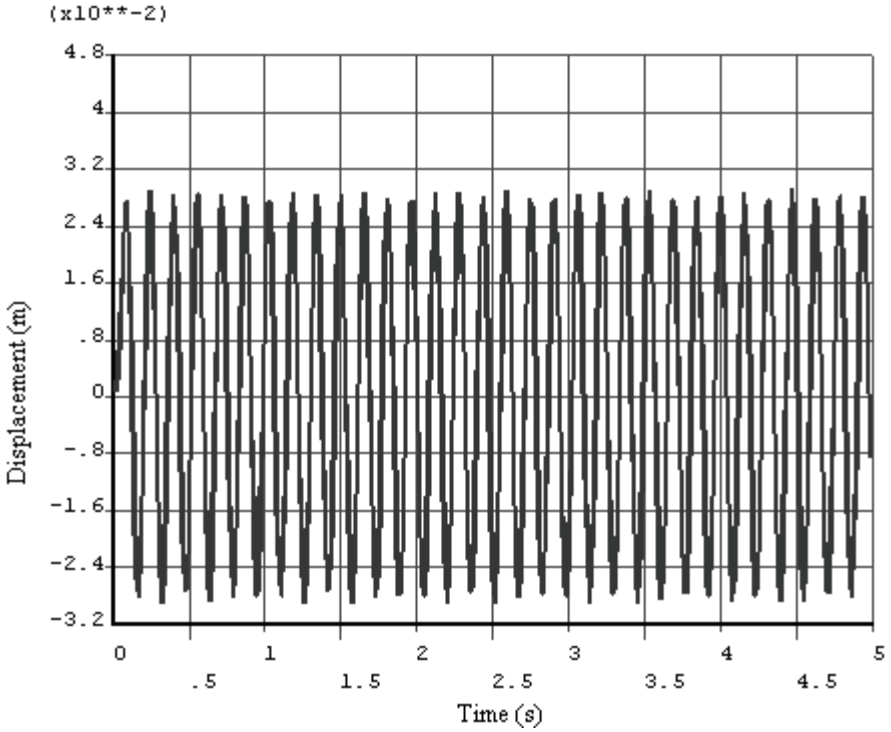

Figure 3.2. Displacement response plot without control

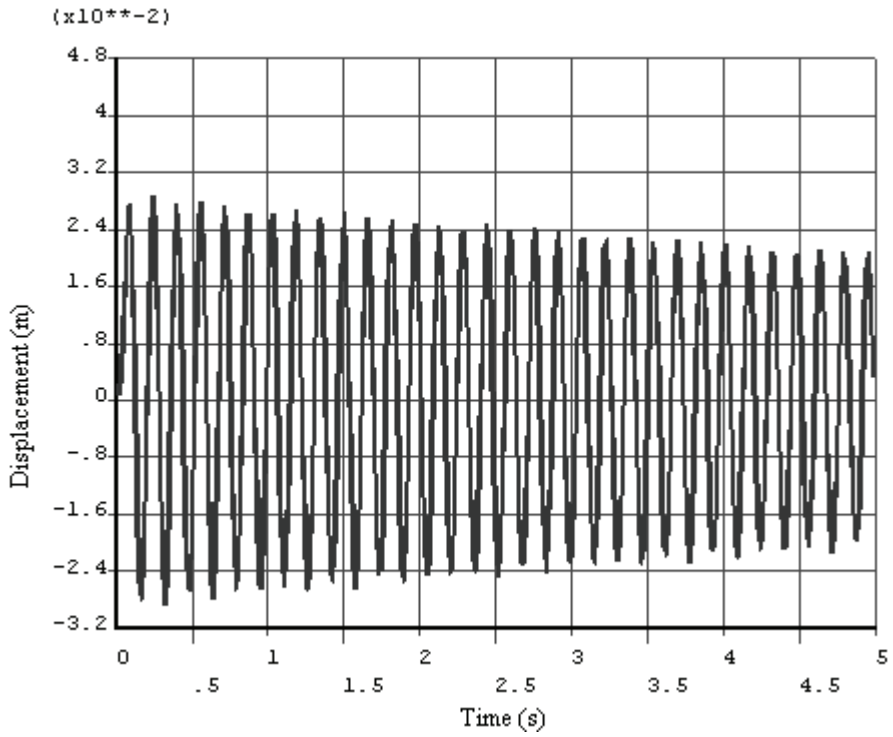

Figure 3.3. Displacement response plot with K_p=25

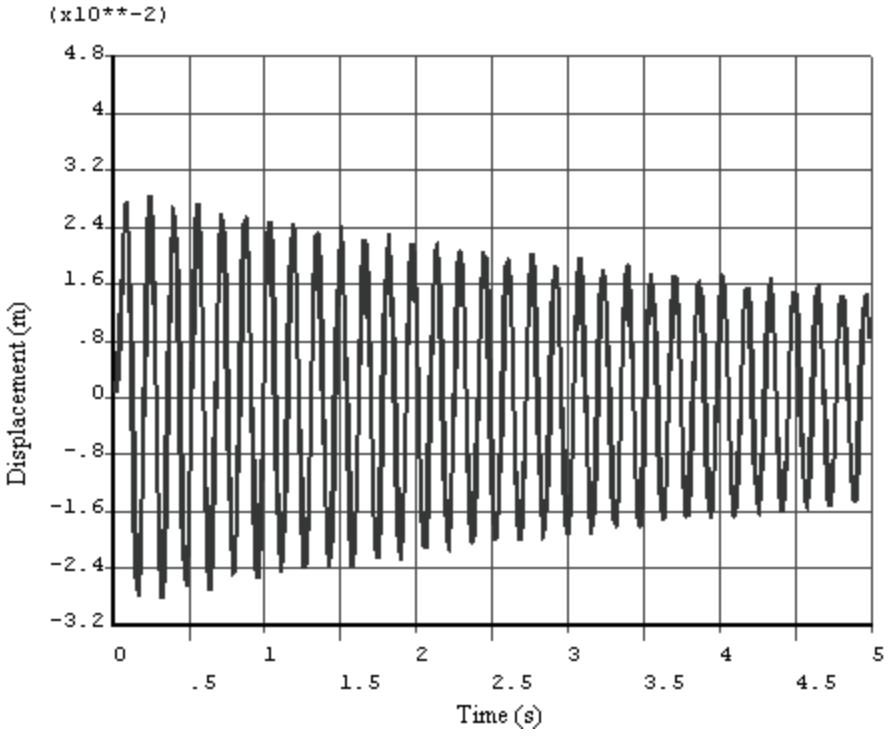

Figure 3.4. Displacement response plot with K_p=50

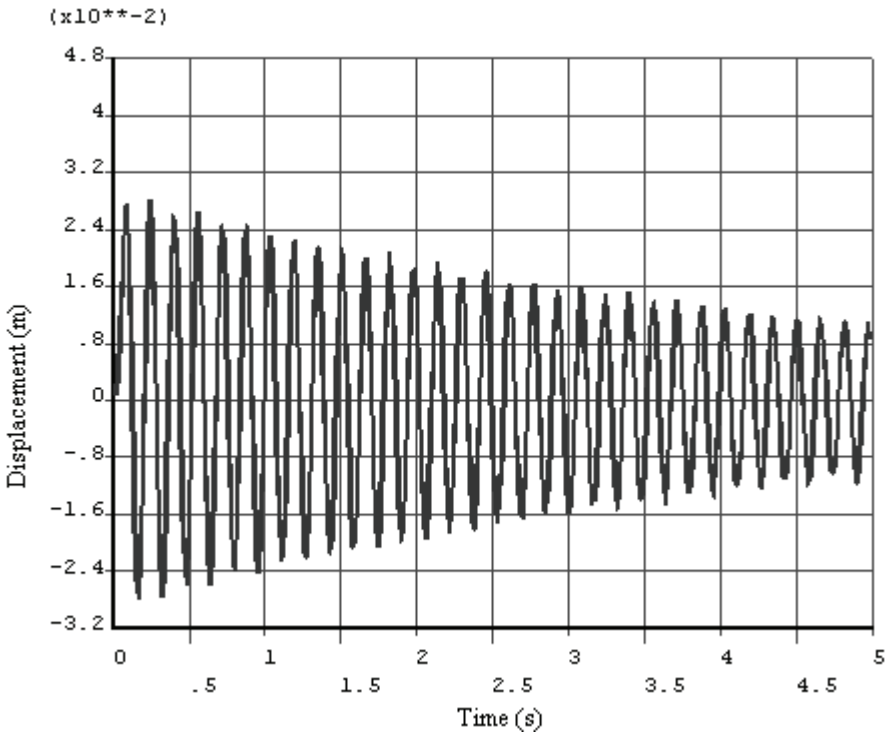

Figure 3.5. Displacement response plot with K_p=75

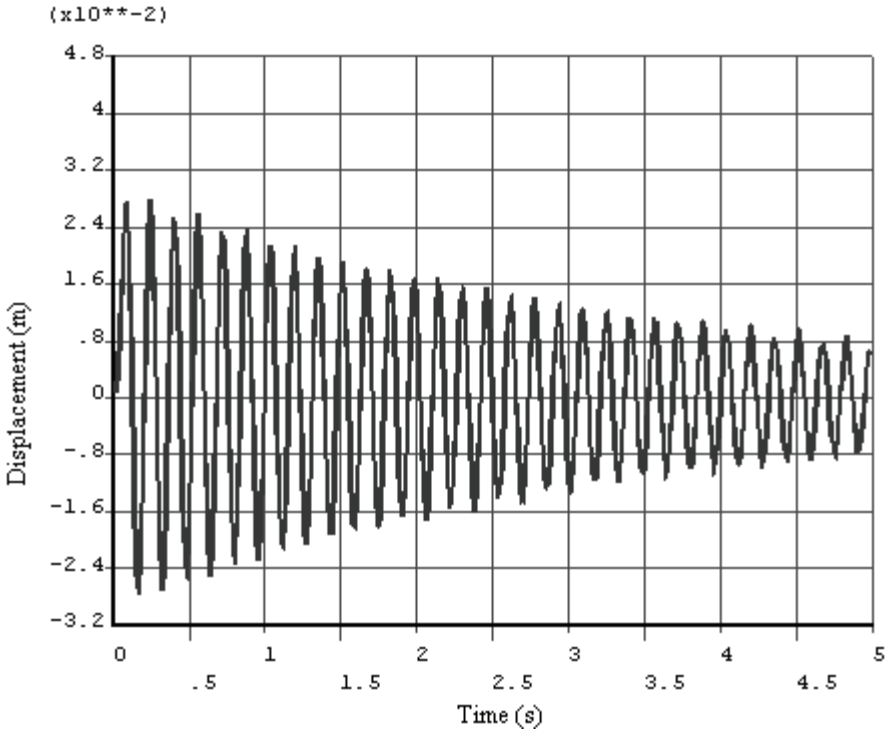

Figure 3.6. Displacement response plot with K_p=100

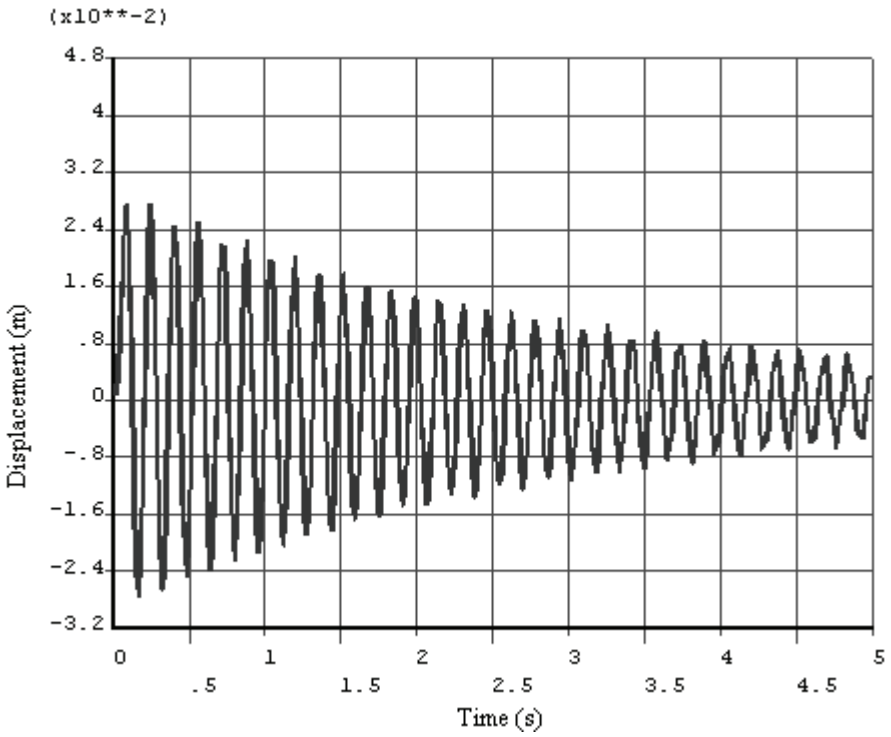

Figure 3.7. Displacement response plot with K_p=125

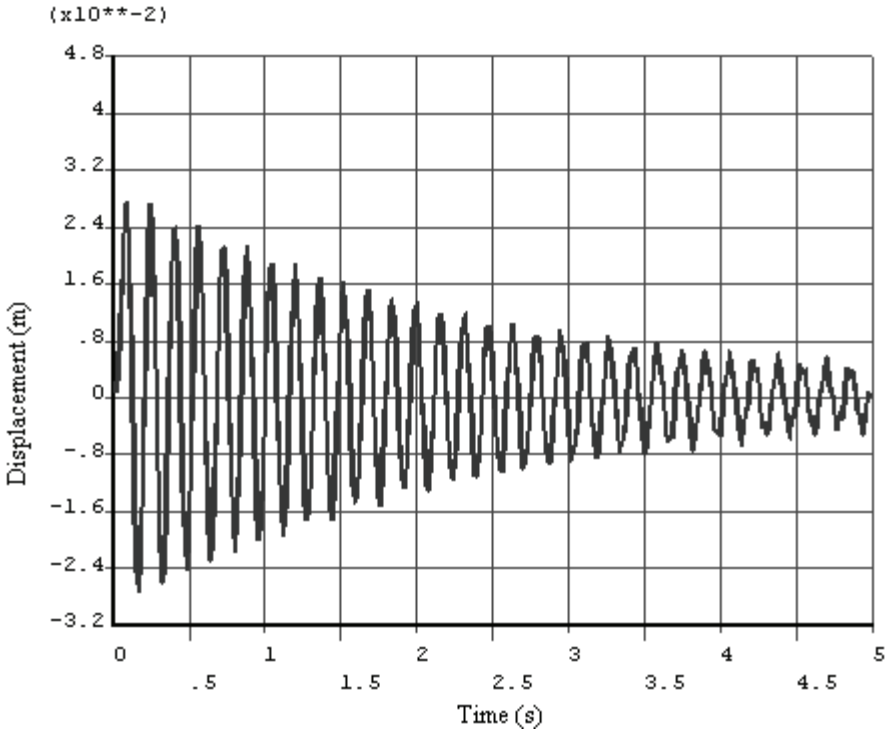

Figure 3.8. Displacement response plot with K_p=150

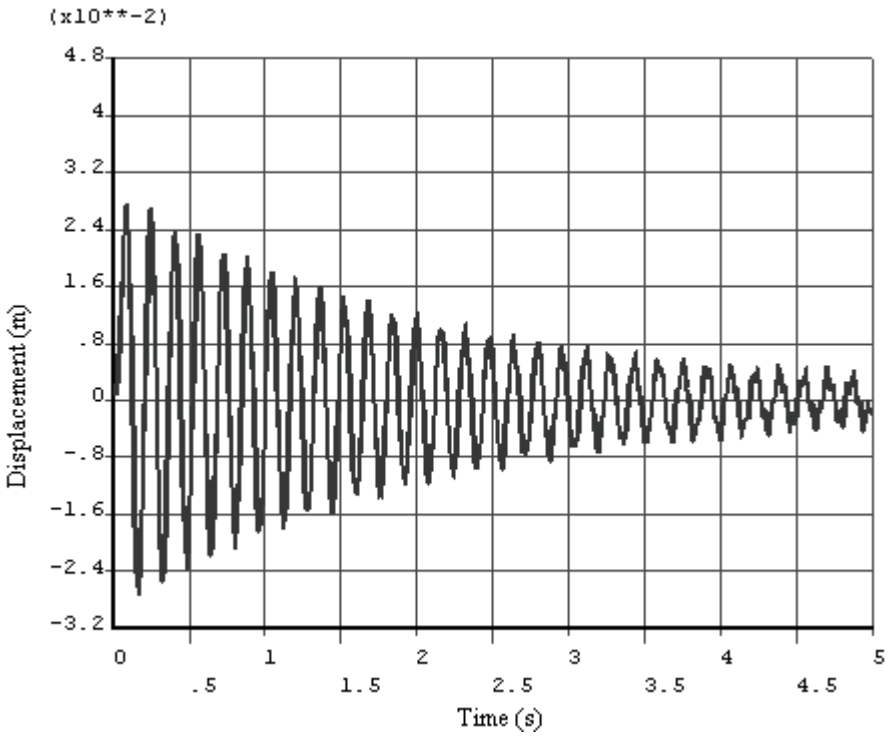

Figure 3.9. Displacement response plot with K_p=175

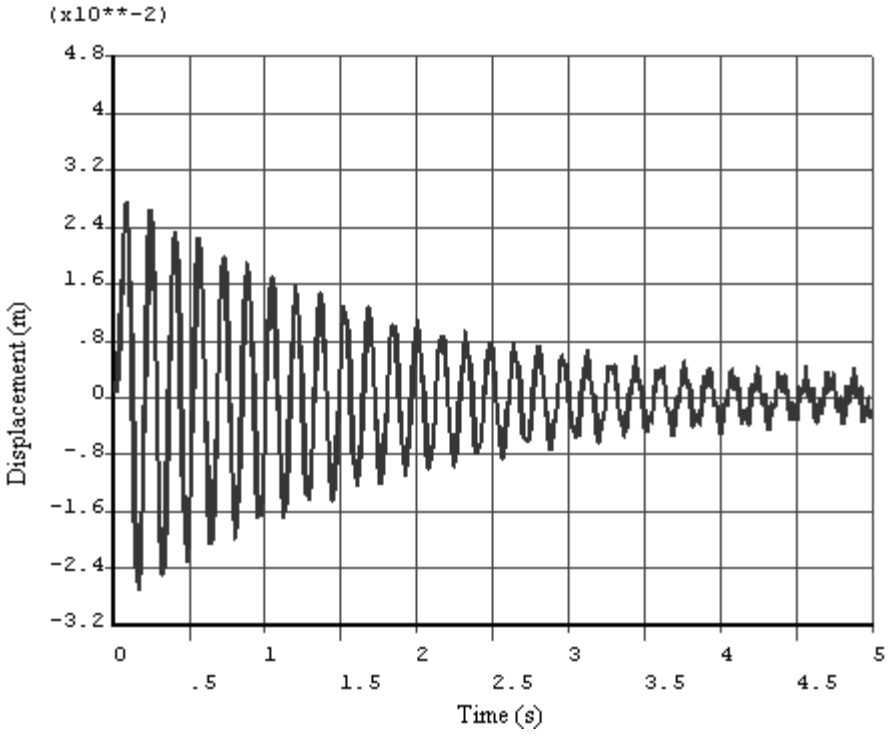

Figure 3.10. Displacement response plot with K_p=200

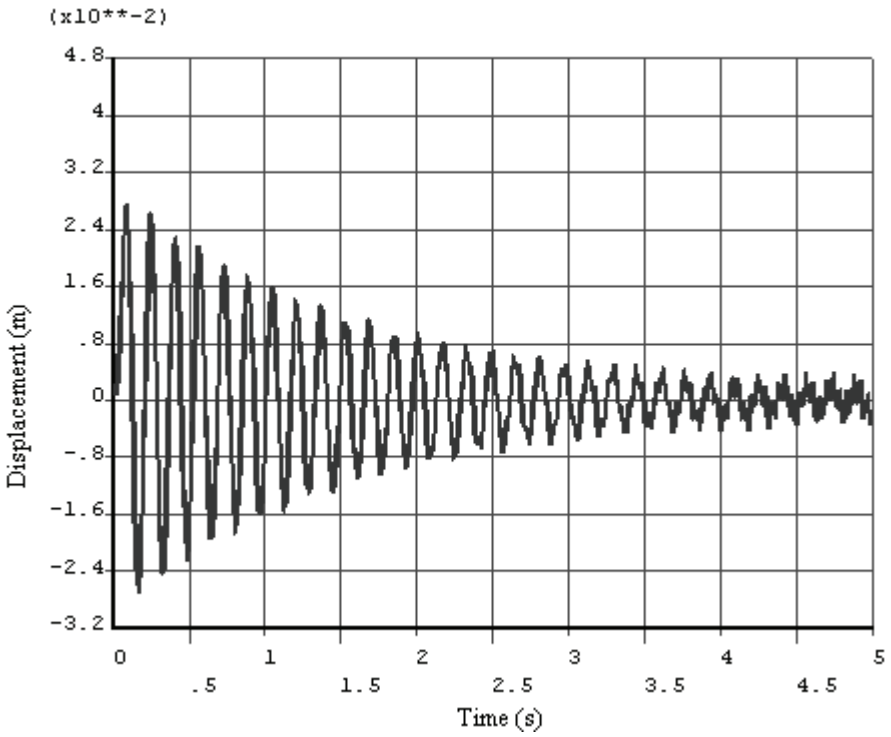

Figure 3.11. Displacement response plot with K_p=225

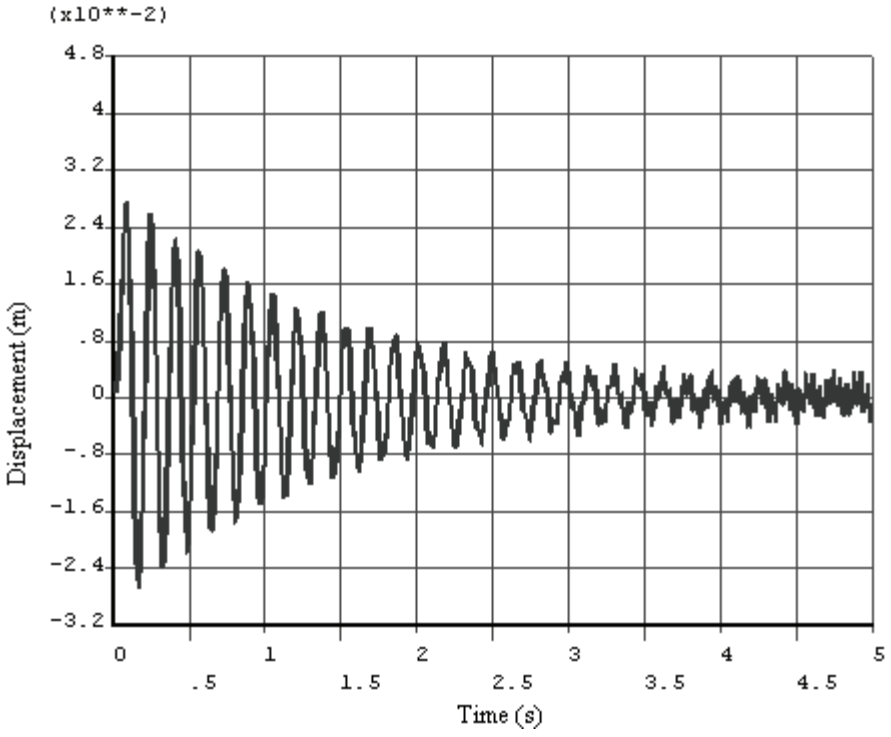

Figure 3.12. Displacement response plot with K_p=250

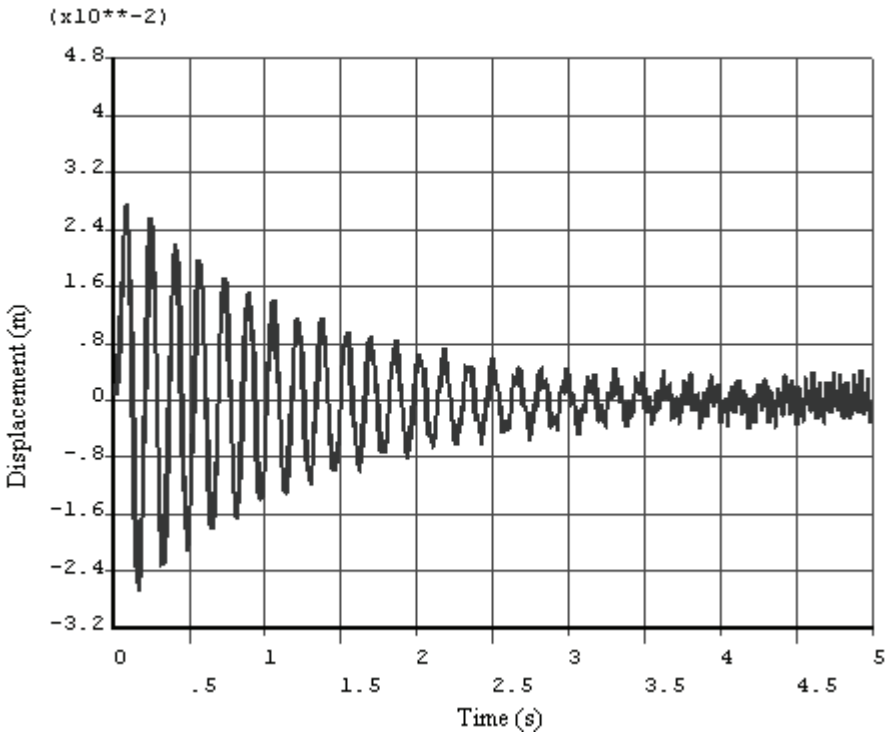

Figure 3.13. Displacement response plot with K_p=275

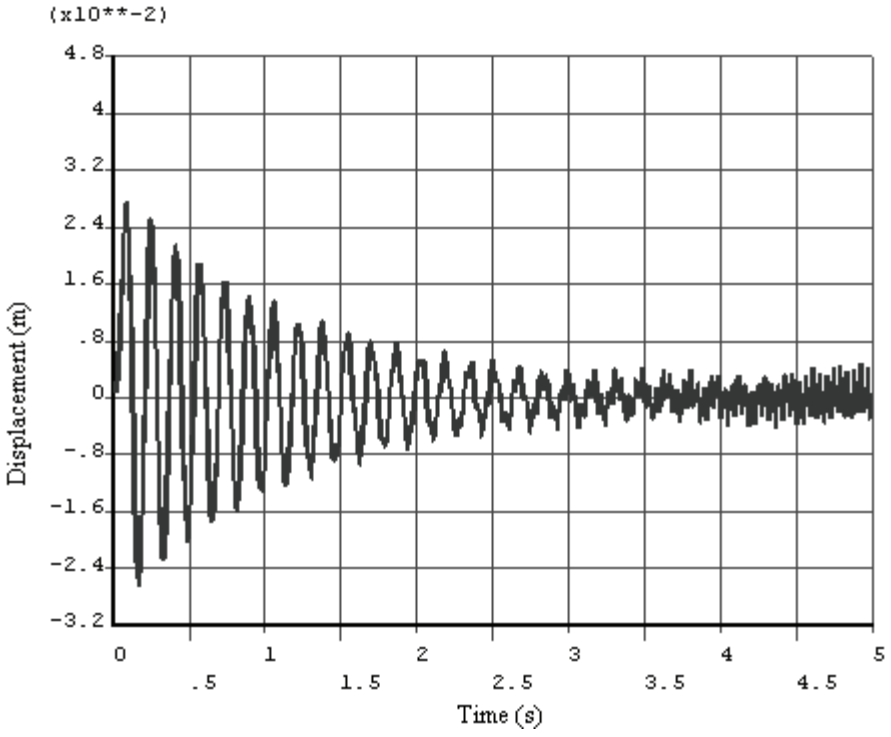

Figure 3.14. Displacement response plot with K_p=300

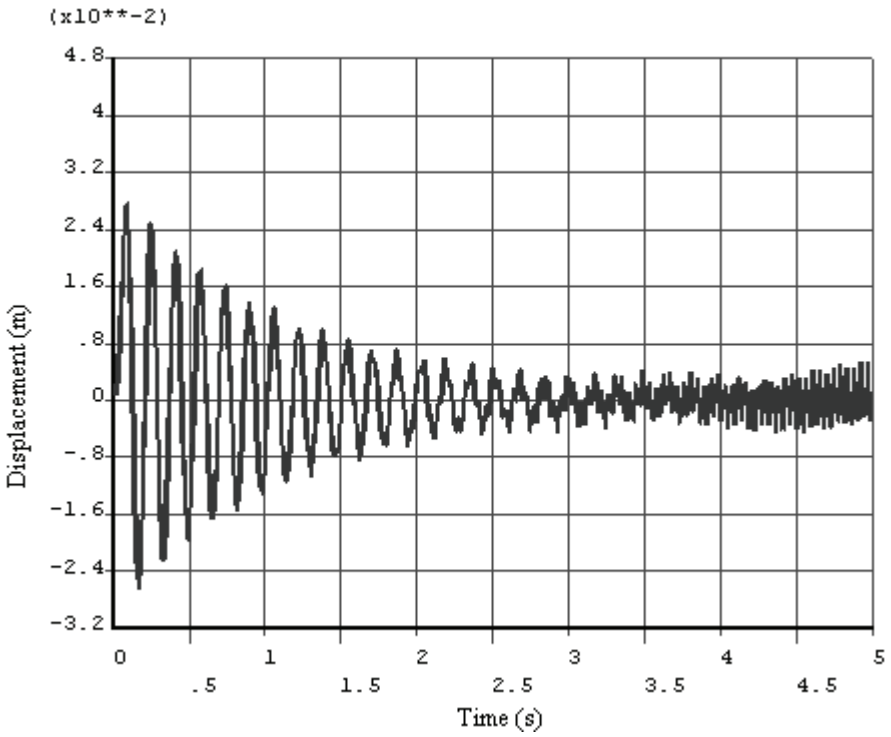

Figure 3.15. Displacement response plot with K_p=325

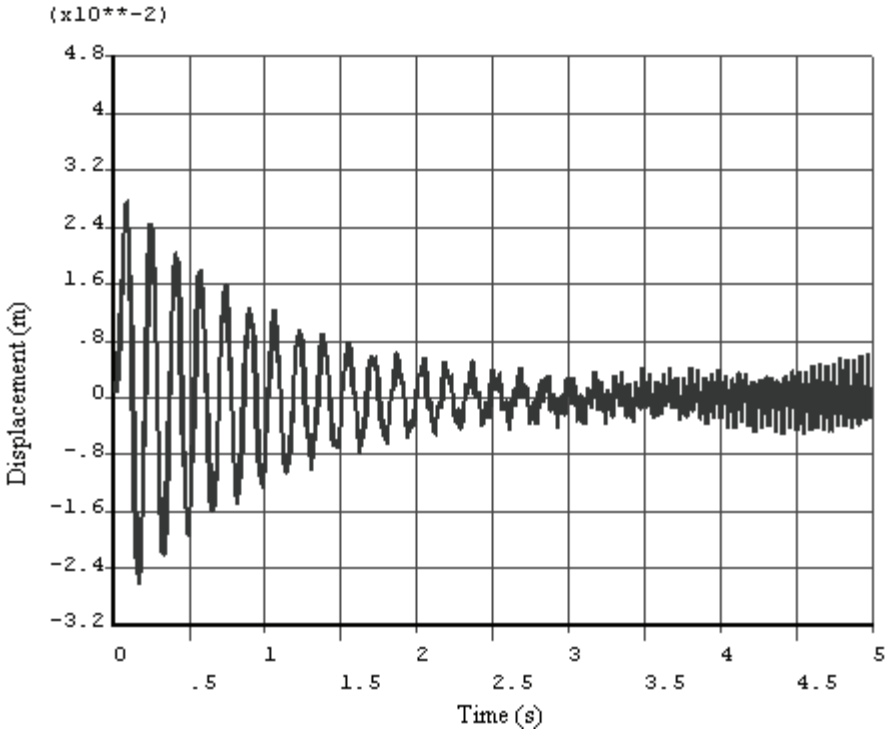

Figure 3.16. Displacement response plot with K_p=350

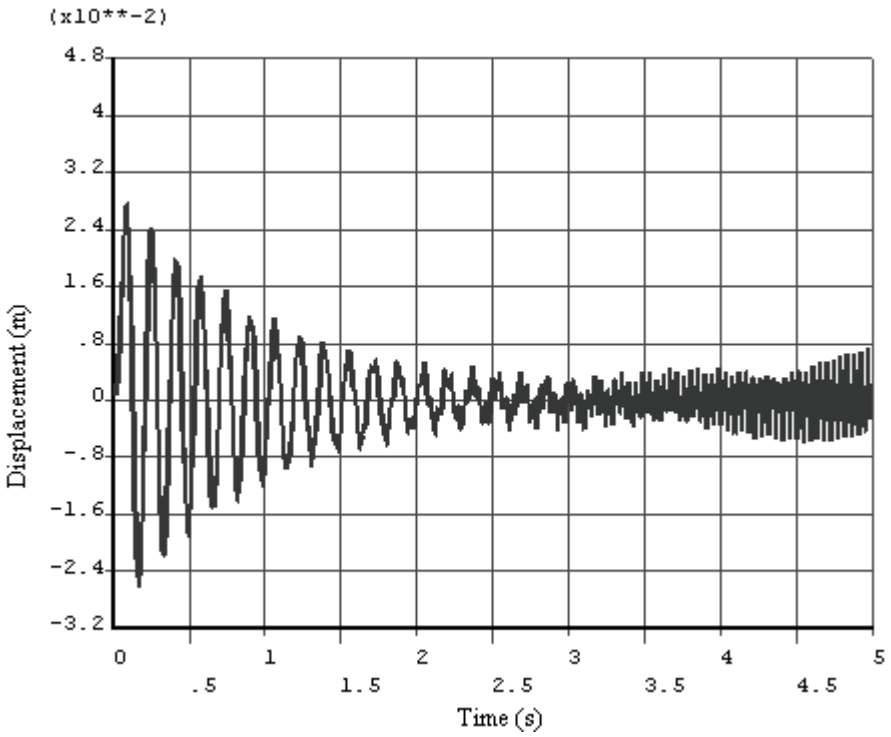

Figure 3.17. Displacement response plot with K_p=375

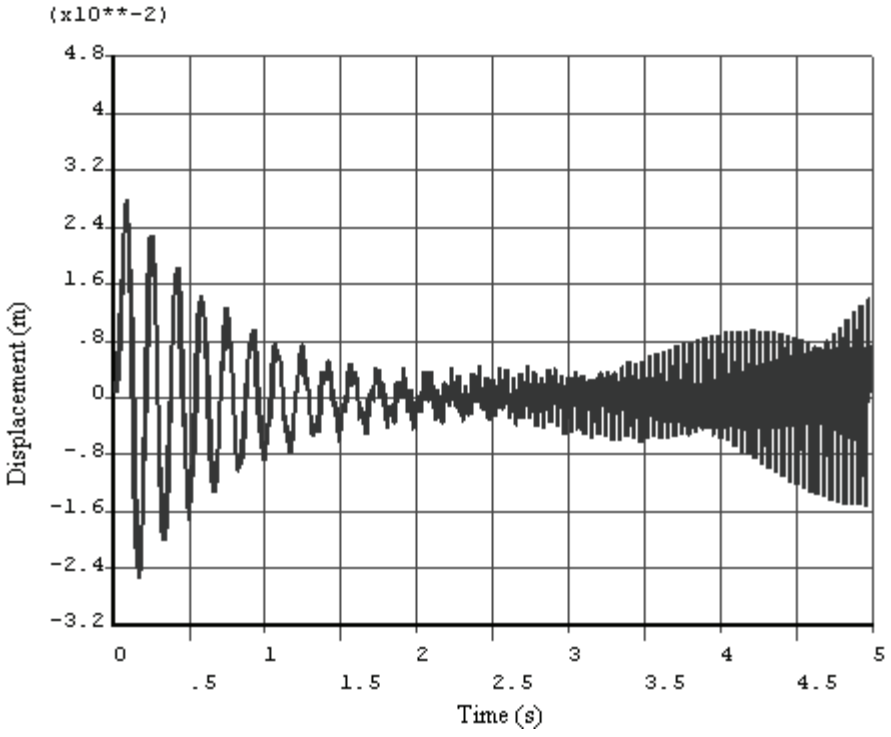

Figure 3.18. Displacement response plot with K_p=500

The feed-back voltage values for the cases presented in Figures 3.2-3.18 are given in the Figures 3.19-3.35.

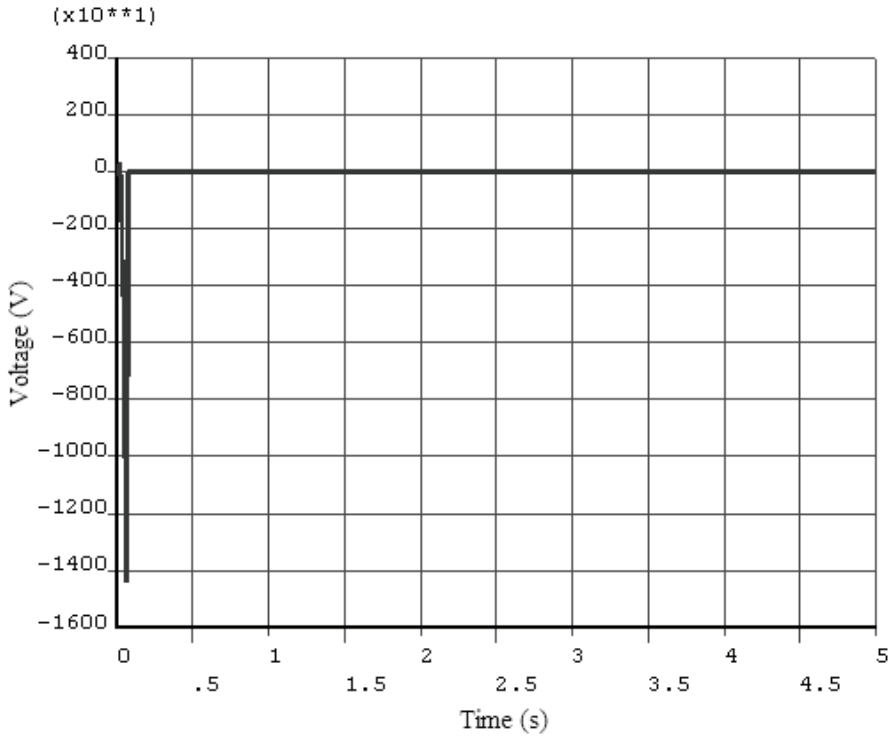

Figure 3.19. Feed-back voltage values for K_p=0.

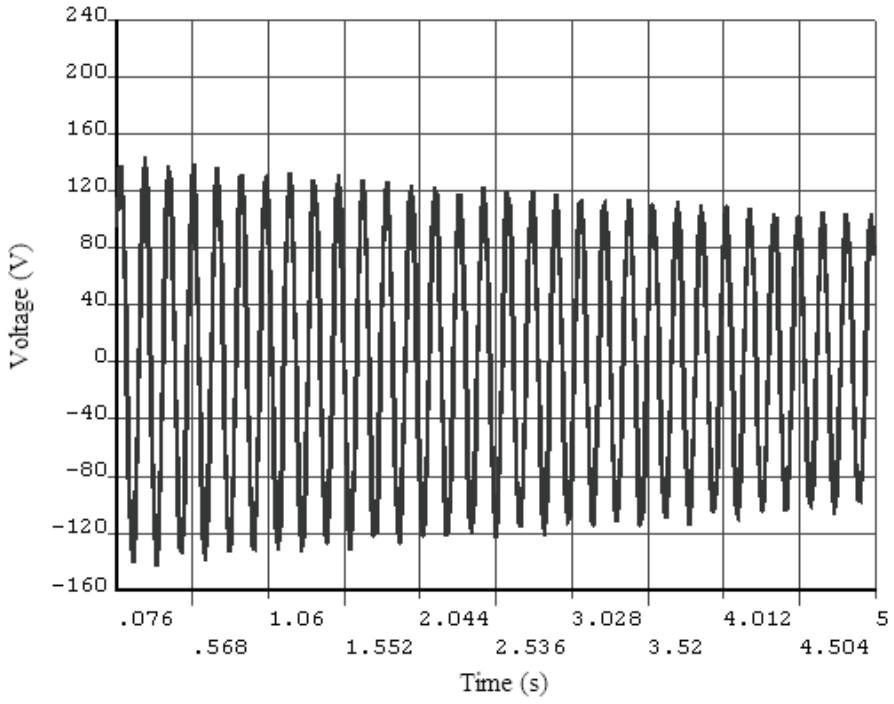

Figure 3.20. Feed-back voltage values for K_p=025

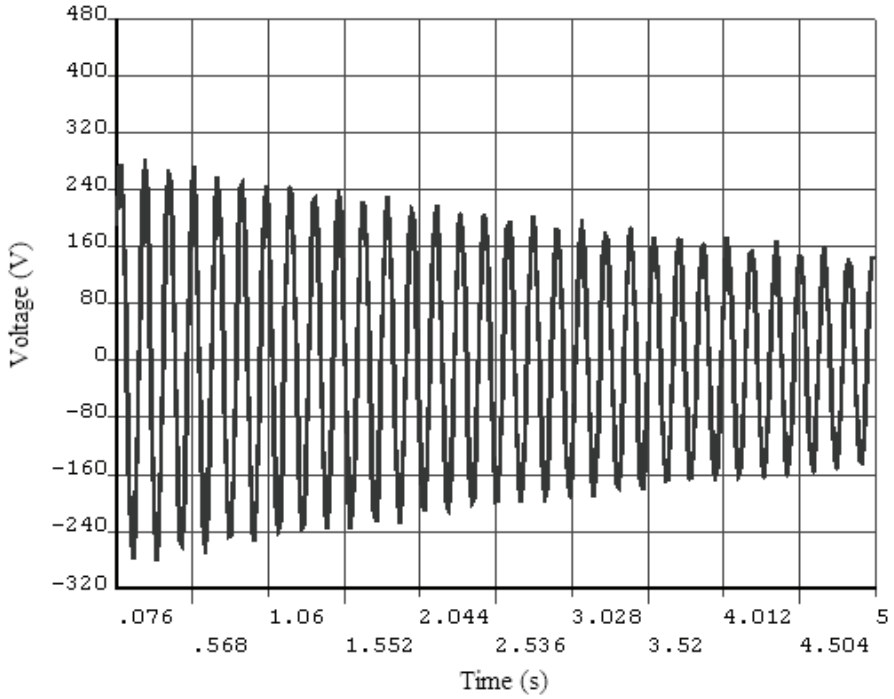

Figure 3.21. Feed-back voltage values for K_p=050

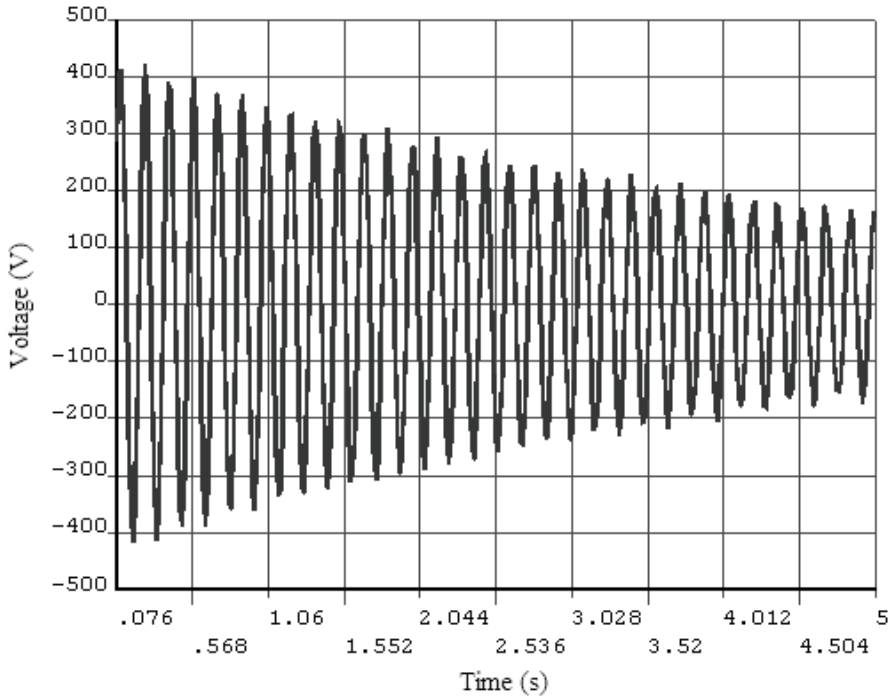

Figure 3.22. Feed-back voltage values for K_p=075

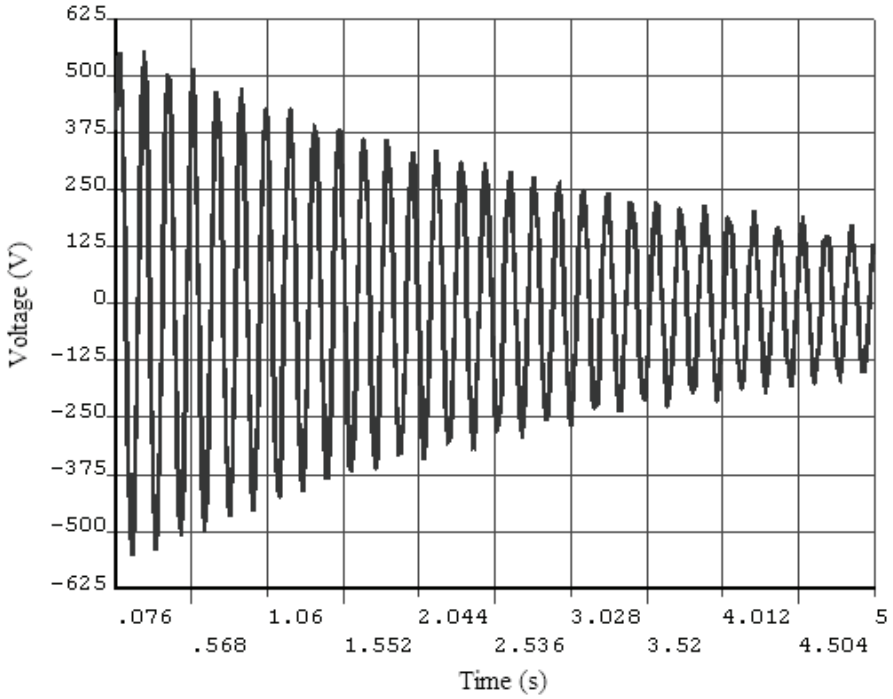

Figure 3.23. Feed-back voltage values for K_p=100

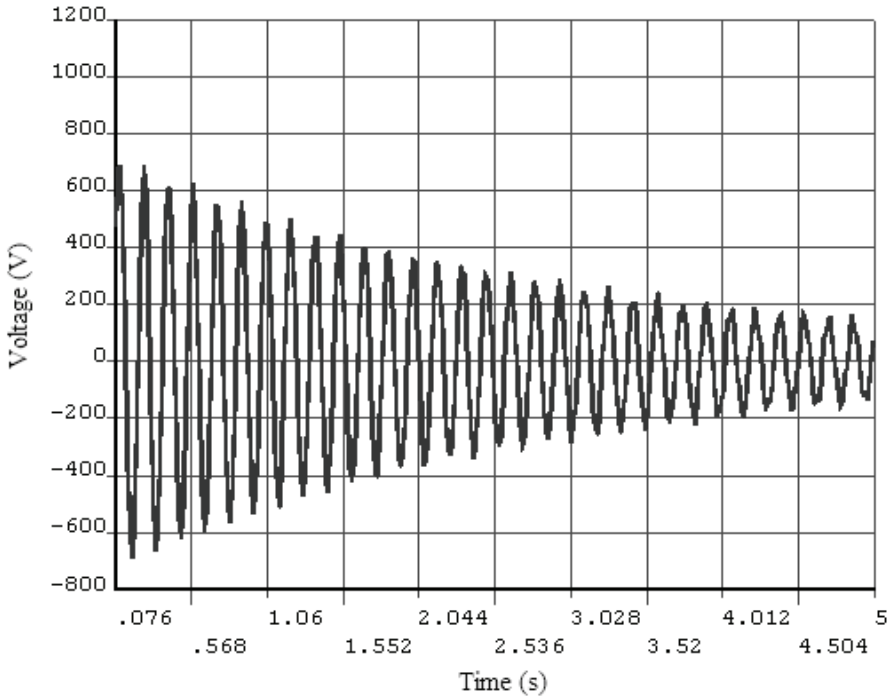

Figure 3.24. Feed-back voltage values for K_p=125

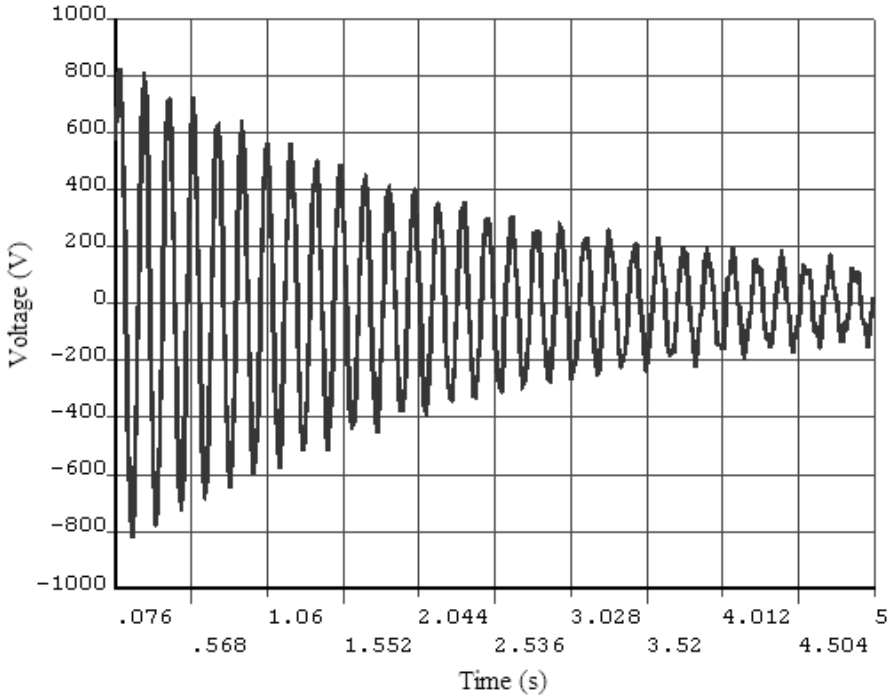

Figure 3.25. Feed-back voltage values for K_p=150

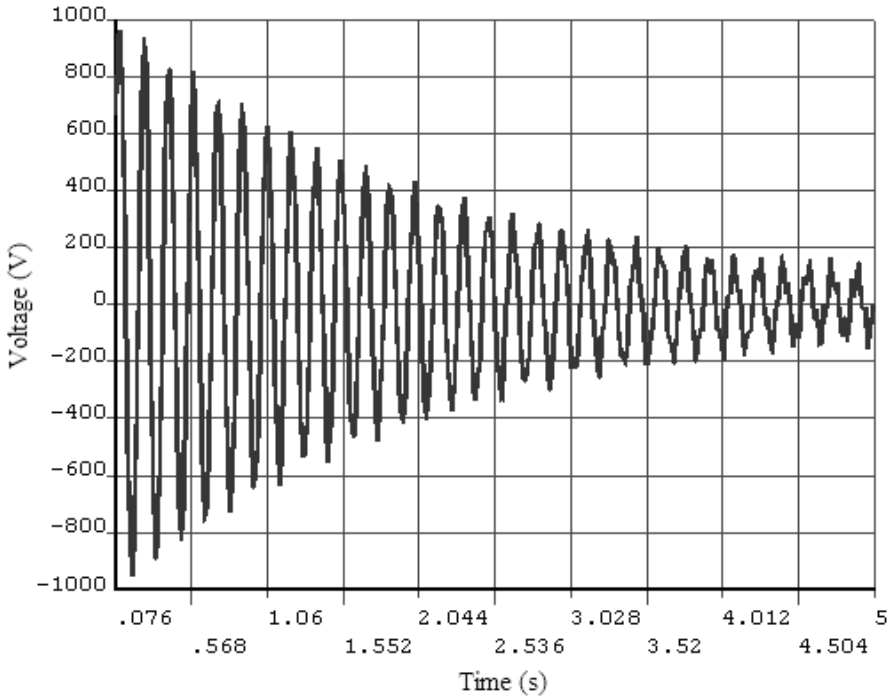

Figure 3.26. Feed-back voltage values for K_p=175

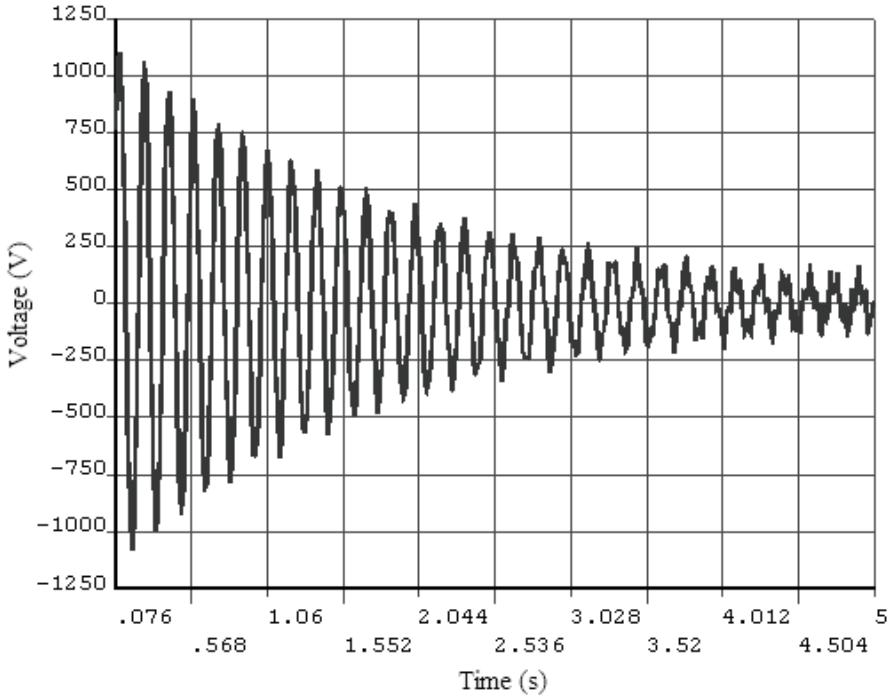

Figure 3.27. Feed-back voltage values for K_p=200

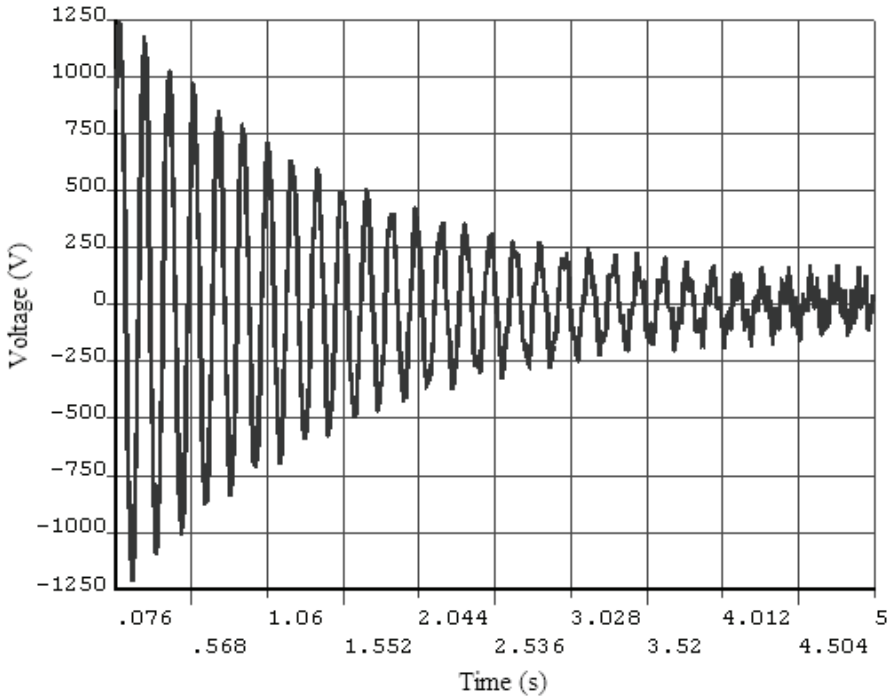

Figure 3.28. Feed-back voltage values for K_p=225

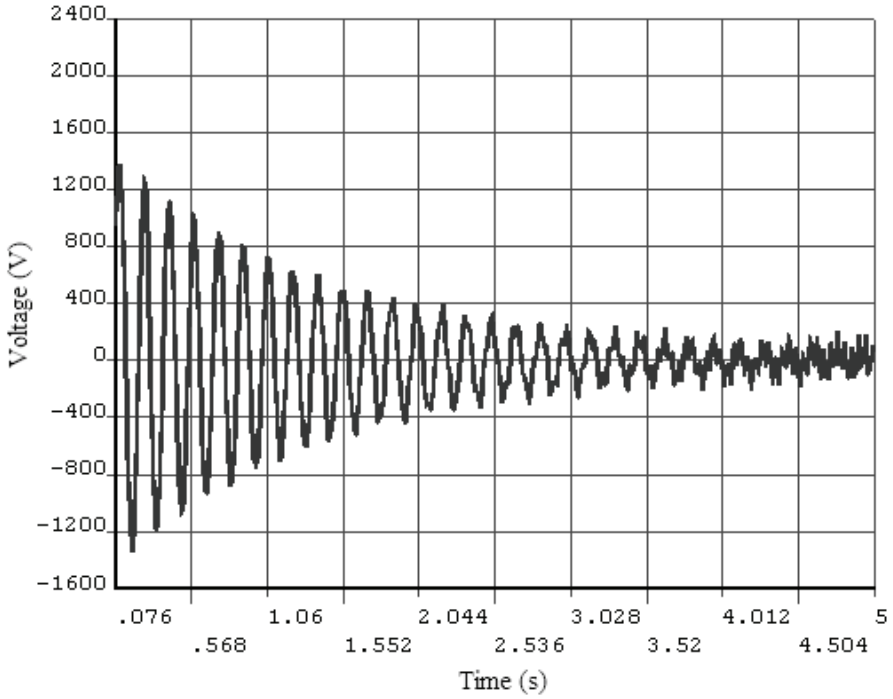

Figure 3.29. Feed-back voltage values for K_p=250

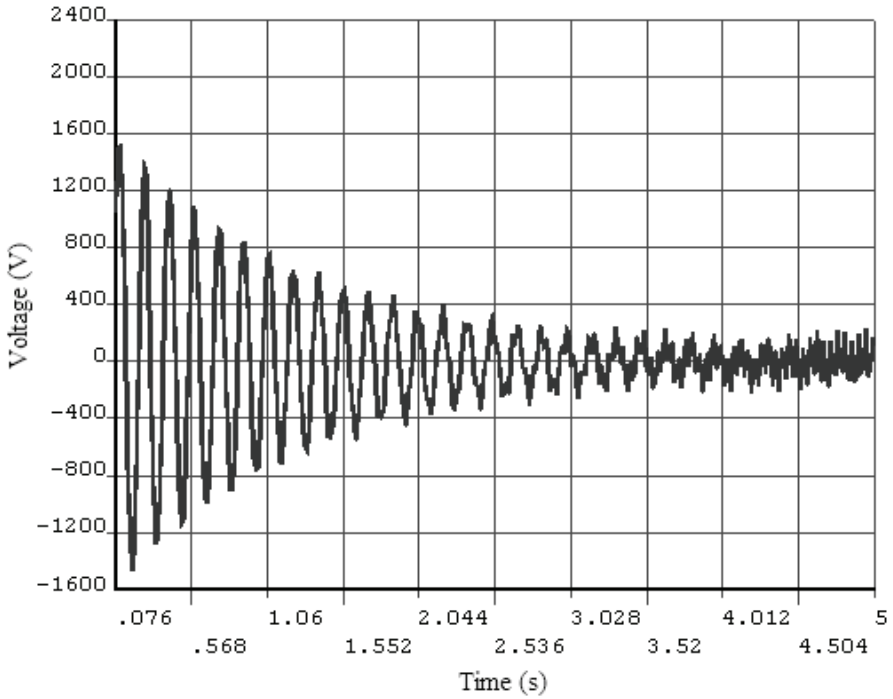

Figure 3.30. Feed-back voltage values for K_p=275

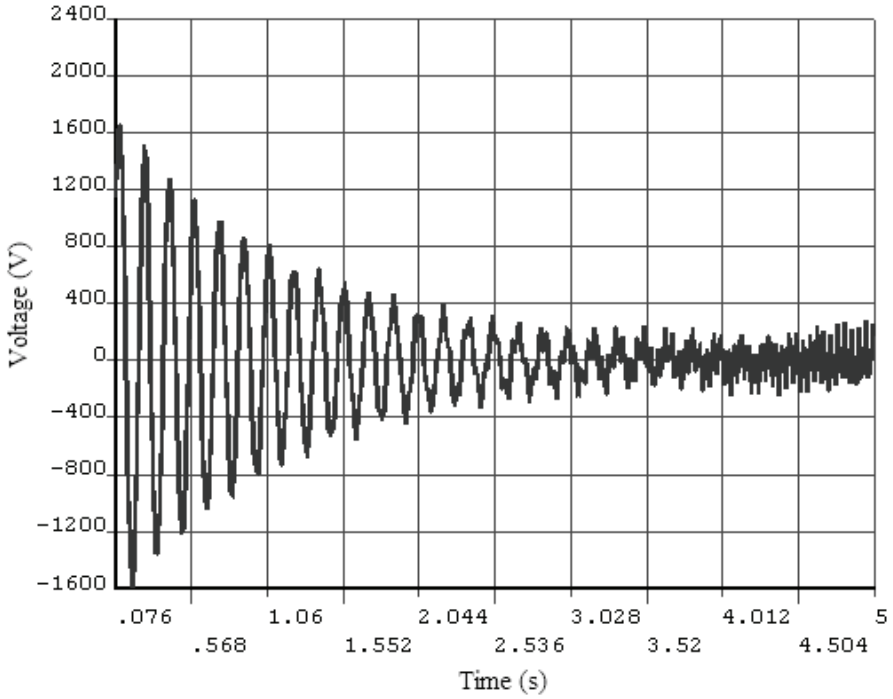

Figure 3.31. Feed-back voltage values for K_p=300

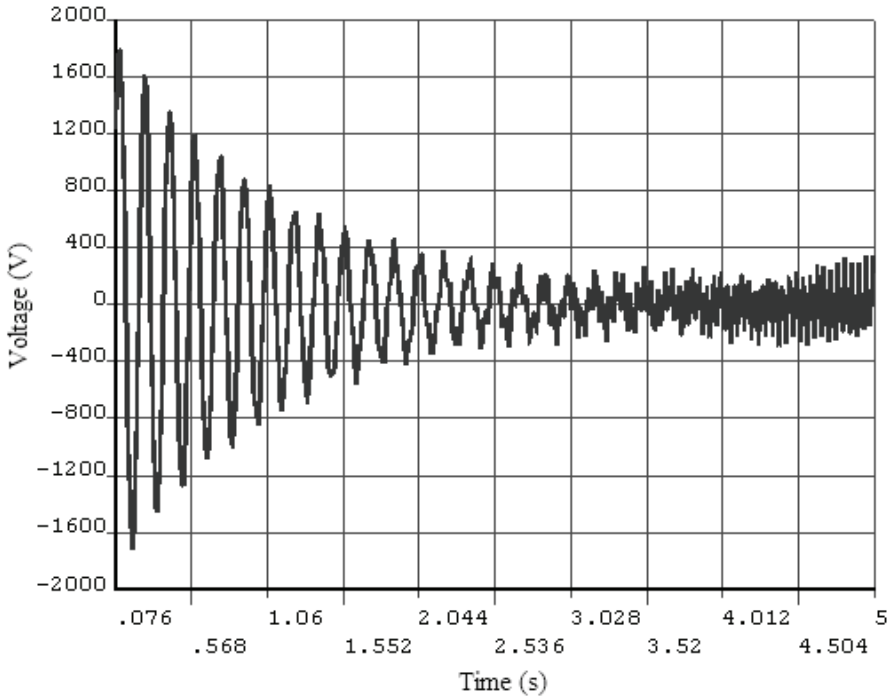

Figure 3.32. Feed-back voltage values for K_p=325

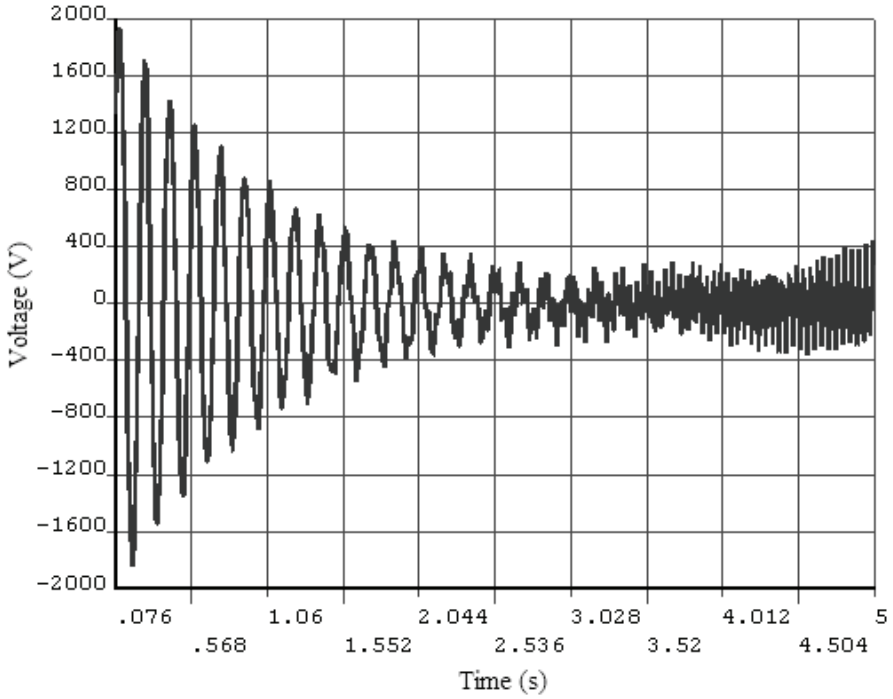

Figure 3.33. Feed-back voltage values for K_p=350

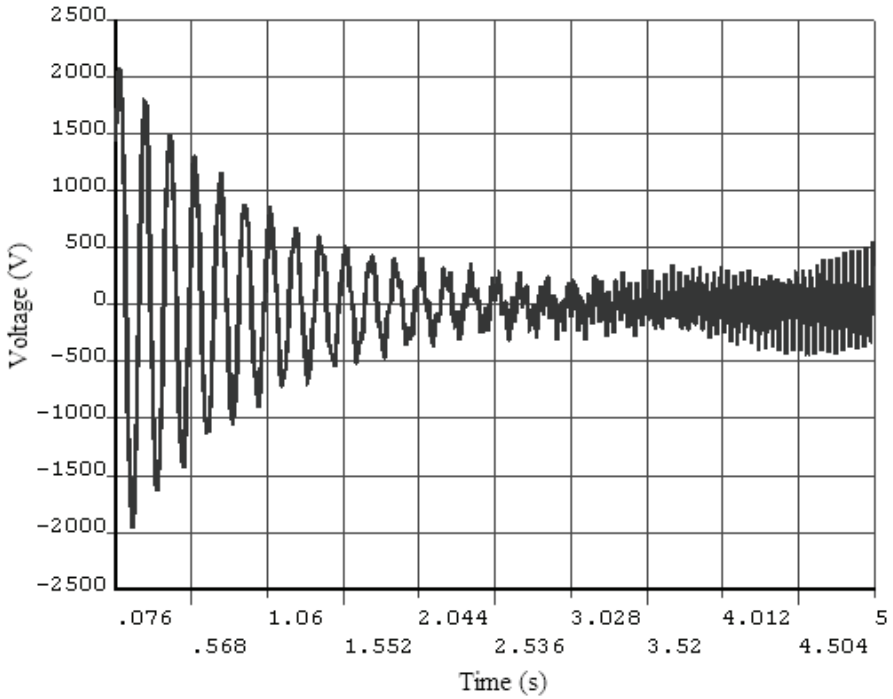

Figure 3.34. Feed-back voltage values for K_p=375

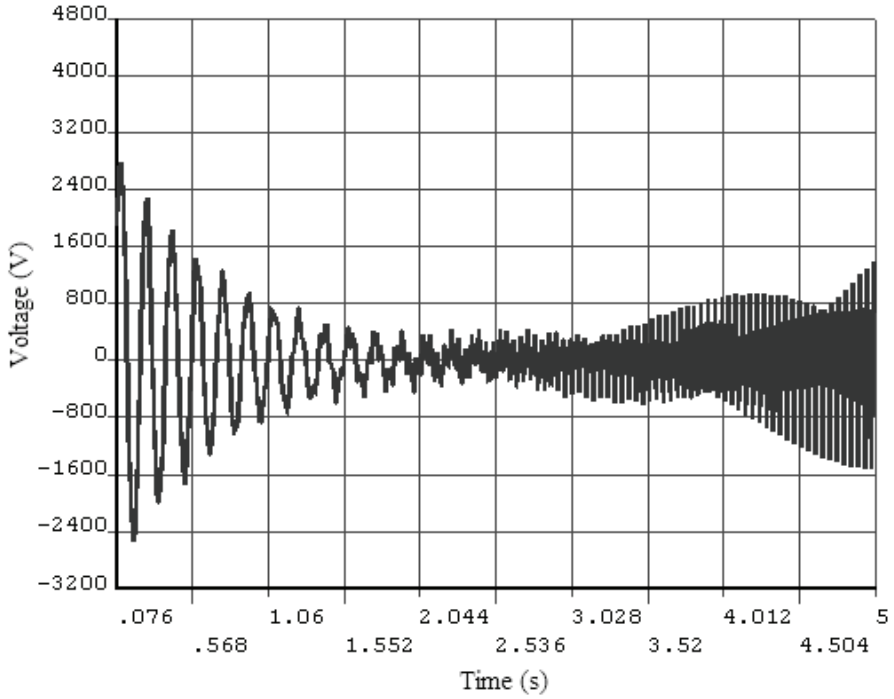

Figure 3.35. Feed-back voltage values for K_p=500

RMS values of the displacement responses for different K_p values for the plots presented in Figures 3.2-3.18 are calculated. These values are given in Table 3.1 and also plotted in Figure 3.36.

Table 3.1. RMS values of the displacement responses for different K_p

K_p	RMS value	K_p	RMS value
0	0.0202	225	0.0085
25	0.0173	250	0.0081
50	0.0151	275	0.0078
75	0.0134	300	0.0075
100	0.0120	325	0.0073
125	0.0110	350	0.0072
150	0.0102	375	0.0071
175	0.0095	500	0.0076
200	0.0089		

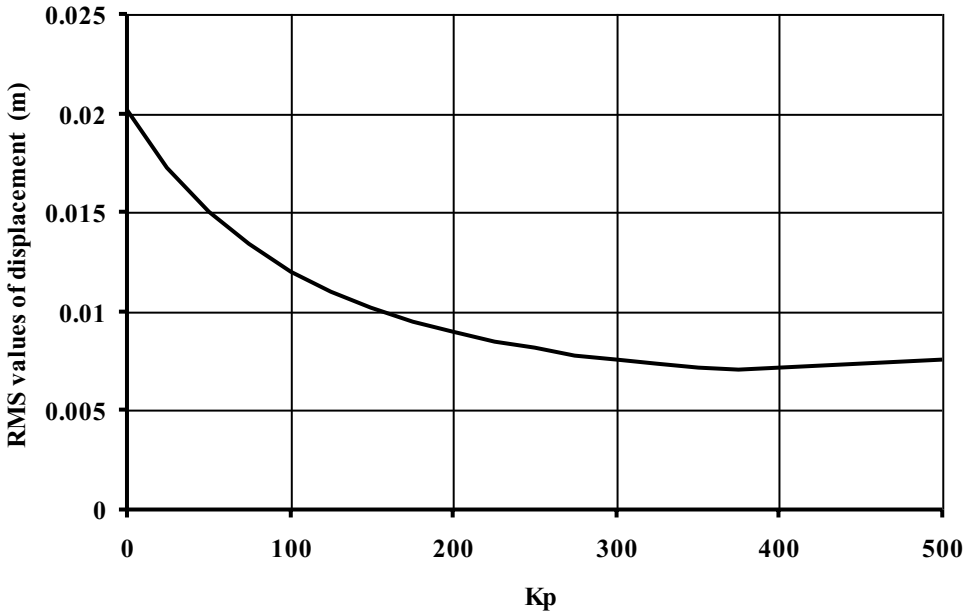

Figure 3.36. RMS values of displacement responses for different K_p values

3.3. Discussion of Results

Active vibration control of smart parabolic curved beam is based on the control parameters which are related with the block diagram given in Figure 2.8.

For numerical method, determination of these parameters is based on trial error method.

By visual evaluation and comparison of the Figures 3.2 through 3.18, it is seen that for K_p values between 25 and 250, the system exhibits a stable behavior, which is evident from the observation that the tip displacement settles within a finite envelope. It is also seen that the settling time decreases as K_p is increased from 25 to 250. The decrease in settling time is valid only until K_p=250 however, after this value, the system starts to become unstable as K_p is increased further. This is observed in Figures 3.13 through 3.18, where the amplitude of the tip displacement is seen as increasing, after an initial duration of declination.

In Figure 3.19, a voltage spike can be seen. This spike occurs due to the strain caused by the application of the initial impulsive force. This force is applied during four time integration steps. One time integration step is determined as one tenths of the first natural period of the smart beam. Since the first natural frequency of the smart beam is 6.60Hz, one time step is calculated as 0.015s. Therefore, four time integration steps

constitute 0.060s. The Figures 3.20 through 3.34 are plotted with the time axis starting from 0.076s in order to leave out this voltage spike.

It can be seen from Figure 3.36 that the RMS values of displacement responses is decreased until a critical value of K_p. However, it is increased after critical value of K_p. Therefore, stability of the system can also be determined from this plot.

CHAPTER 4

CONCLUSIONS

There are numerous studies on vibration control of curved beams with piezoelectric layers in the existing literature. However, researches on vibration control of non circular smart curved beam are rare.

Since the present problem is represented mathematically by differential eigenvalue problem with variable coefficients which has solution only for special cases of functions of the variable coefficients, Finite Element Method is used to reduce the differential eigenvalue problem to discrete eigenvalue problem. A computer code is developed in ANSYS to model the geometry and solve the vibration control problem by using APDL (ANSYS Parametric Design Language). Vibration control is performed by displacement feed-back algorithm. The effects of control parameters on time response are investigated.

REFERENCES

Archer, R.R. 1960. Small vibrations of thin incomplete circular rings. *International Journal of Mechanical Science* 1: 45-56.

Auld, B.A., 1973. Acoustic Fields and Waves in Solids, Volume I. New York: John Wiley & Sons, Inc.

Banks, H.T. and Zhang, Y., 1997. Computational methods for a curved beam with piezoelectric patches, *Journal of Intelligent Material Systems and Structures* 8: 260-278.

Brei, D.E., and Blechschmidt, J. 1992. Design and static modeling of a semiconductor polymeric piezoelectric microactuator. *Journal of Microelectromechanical Systems* 1(3): 106–115.

Brei, D.E. 1995. Design and development of a new class of piezoelectric actuators for force improvement. Active Materials and Smart Structures, College Station, Texas, United States, 343–356.

Henrych, J., 1981. The Dynamics of Arches and Frames, Amsterdam, Elsevier.

IEEE, 1988, IEEE Standard on Piezoelectricity, Std. 176-1987, Piscataway, New Jersey: IEEE.

Kohnke, P., 2004. ANSYS, Inc. Theory Reference. Canonsburg: ANSYS, Inc. online documentation or the ANSYS

Kuang, Y.D., Li, G.Q., Chen, C.Y., and Min, Q., 2007. The static responses and displacement control of circular curved beams with piezoelectric actuators, *Smart Materials and Structures* 16:1016–1024.

Love, Augustus E.H. 1944. A treatise on the mathematical theory of elasticity. New York: Dover Publications.

Moskalik, A.J. and Brei, D., 1997. Deflection-voltage model and experimental results for polymeric piezoelectric C-Block actuators, *AIAA Journal* 35: 1556-1448.

Preumont, A., 2002. Vibration Control of Active Structures. Second edition. New York: Kluwer Academic Publishers.

Shih, H.R., 2000. Distributed vibration sensing and control of a piezoelectric laminated curved beam, *Smart Materials and Structures* 9: 761–766.

Sun, D. and Tong, L., 2002. Modeling and analysis of curved beams with debonded piezoelectric sensor/actuator patches, *International Journal of Mechanical Sciences* 44: 1755–1777.

Yoon, H.-S., Washington, G., and Danak, A. 2005. Modeling, optimization, and design of efficient initially curved piezoceramic unimorphs for energy harvesting applications. *Journal of Intelligent Material Systems and Structures* 16(10): 877–888.

Wang, R.T., 2010. Structural responses of surfac-mounted piezoelectric curved beams, *Journal of Mechanics* 26: 439-451.

Yardimoglu, B., 2012. Lecture notes on Finite Element Method, Izmir: Izmir Institute of Technology.